SLAC-PUB-7627
August 1997

GASEOUS WIRE DETECTORS*

J. Va'vra
Stanford Linear Accelerator Center, Stanford University,
Stanford, CA 94309, U.S.A.

Abstract

This article represents a series of three lectures describing topics needed to understand the design of typical gaseous wire detectors used in large high energy physics experiments; including the electrostatic design, drift of electrons in the electric and magnetic field, the avalanche, signal creation, limits on the position accuracy as well as some problems one encounters in practical operations. Reader should also refer to Ref. 1-4.

Chapter 1

1.1. Two-dimensional electrostatic field in a drift cell

This lecture will cover the following topics:

a) numerical solution for wires only,

b) analytical solution for wires and pads,

c) numerical solution for any shape of electrodes,

d) numerical solution for wires, pads and dielectric.

We start the lecture by reminding the **Gauss law in the integral form**:

$$\Phi = \oint_S \vec{E} \cdot d\vec{S} = \frac{1}{\varepsilon_r \varepsilon_0} \sum_i Q_i \qquad (1.1)$$

where $\sum Q_i$ is sum of all charges within the volume defined by surface S, Φ is total flux of electric field $\vec{E}$ through surface S, ε_r is effective relative dielectric constant, $\varepsilon = \varepsilon_r \varepsilon_0$ is the dielectric constant of the medium within the surface S and $\varepsilon_0 = 8.85$ pF/m is permitivity of free space.

1.2. Two-dimensional electrostatic field (wires only, no dielectric)

Example #1- Find the potential and the electric field of an infinitely long charged line with charge per unit length λ (surface S is defined a cylinder of length L and radius r; $\varepsilon_r = 1$):

$$\Phi = 2\pi r L E = \frac{\lambda L}{\varepsilon_0} \qquad (1.2)$$

---

* Lectures given at ICFA Instrumentation School, Guanajuato, Mexico, June 7-18, 1997.

Work supported in part by US Department of Energy under contract DE-AC02-76SF00515.

The potential distribution V(r) is then:

$$V(r) = -\int E(r)\, dr = -\frac{\lambda}{2\pi\varepsilon_0}\int \frac{dr}{r} = -\frac{\lambda}{2\pi\varepsilon_0}\ell n\, r + C \qquad (1.3)$$

To determine the linear charge λ, we need a boundary condition. This is done by relating the wire voltage V_o and the linear charge λ on the surfaces of the conductor, such as a grounded tube surrounding the wire (r_a is anode wire radius, r_c is cathode tube radius):

$$V_0 = \int_{r_a}^{r_c} \vec{E}.d\vec{r} = \frac{\lambda}{2\pi\varepsilon_0}\ell n\frac{r_c}{r_a} \qquad (1.4)$$

The electric field on the surface of the wire with radius r_a is then:

$$E_a = \frac{1}{2\pi\varepsilon_0}\frac{\lambda}{r_a} \qquad (1.5)$$

In case of anode wire, E_a will be used to estimate the wire gain. Typical values of the electric field on the anode wire surface is 200-400 kV/cm; whereas on the cathode wire surface it is less than 20 kV/cm.

Example #2 - Determine the electric gradient on the surface of cathode wires:

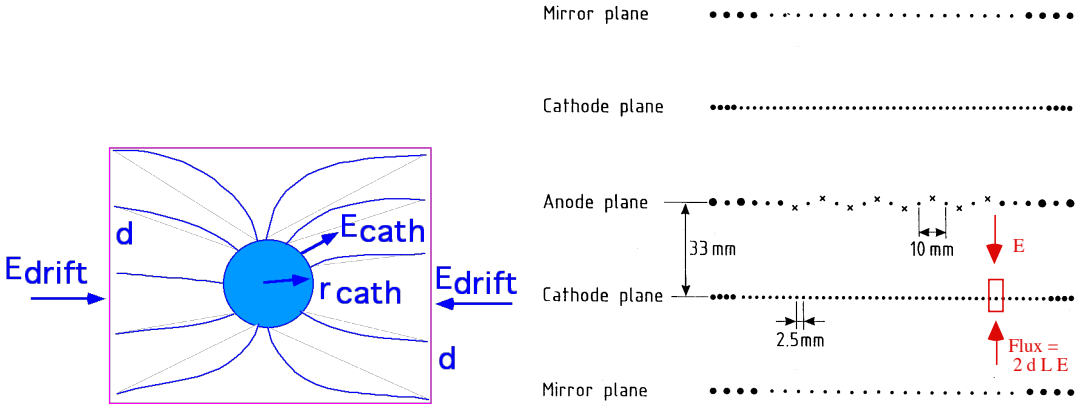

Fig.1 - Geometry of the drift cell; cathode plane is made of 100 μm dia. Cu-Be wires separated by d = 2.5 mm gap; drift field is E = 950 V/cm, wire length L.

The field lines in the middle of drift cell have to end on the cathode wire charges. Therefore field flux $\Phi = 2\, d\, L\, E_{drift\ field} = \lambda\, L/\varepsilon_0 = 2\, L\, \pi\, R_{cath.}\, E_{cathode\ wire\ radius}$ and $E_{cathode\ wire\ radius} = d\, E_{drift\ field}/(\pi\, r_{cath.}) = 0.25 \times 950/(\pi\ 50 \times 10^{-4}) \sim 15.1$ kV/cm.

Example #3 - Determine the two-dimensional potential and electric field in the drift cell.

Input variables: V_i - voltages on each wire, i = 1,..N

$\vec{r}_i$ - wire positions, i = 1,...N

a_i - wire radii, i = 1,...N

L - length of the wire

Output variables: λ_i - charge per unit length, i = 1,...N

Using the **superposition principle** and the **Gauss law** (see Example #1), the potential at any point within the cell is a result of a summation of potentials resulting from individual linear charges on the wires:

$$V(\vec{r}) = \frac{1}{2\pi\varepsilon_0} \sum_{k=1}^{N} P_{ik}\, \lambda_i\,, \quad \vec{r} \neq \vec{r}_i \tag{1.8}$$

where P_{ik} are called **potential coefficients**:

$$P_{ik} = \ell n\left(\left|\vec{r}_i - \vec{r}_k\right|\right),\ i \neq k \tag{1.9}$$
$$P_{ii} = \ell n(a_i)$$

This method is quite general - it can be applied to calculate the potential for charges of any type (point, line, ring, etc.). To determine the linear charges λ_k, we need a boundary condition. This is done by relating the wire voltages V_i and the linear charges λ_k on the surfaces of conductors:

$$V_i = \frac{1}{2\pi\varepsilon_0} \sum_{k=1}^{N} P_{ik}\, \lambda_k \tag{1.10}$$

In addition, one can assume that the total charge of the system is zero $\sum_{i=1}^{N} \lambda_i = 0$.

One can rewrite the equation (1.10) in the matrix form:

$$\begin{pmatrix} 0 \\ V_1 \\ \cdot \\ V_N \end{pmatrix} = \frac{1}{2\pi\varepsilon_0} \begin{pmatrix} 0 & 1 & \cdot & 1 \\ 1 & \cdot & \cdot & \cdot \\ \cdot & \cdot & P_{ik} & \cdot \\ 1 & \cdot & \cdot & \cdot \end{pmatrix} \begin{pmatrix} \lambda_0 \\ \lambda_1 \\ \cdot \\ \lambda_N \end{pmatrix} \tag{1.11}$$

input known unknown

Solution is:

$$\lambda_i = 2\pi\varepsilon_0 \sum_{k=1}^{N} C_{ik}\, V_k \tag{1.12}$$

where C_{ii} are called coefficients of capacitance and C_{ik}, $i \neq k$ are called coefficients of induction. Once we know the linear charges λ_i on each wire, the potential and electric field in space anywhere between the wires is given by:

$$V(\vec{r}) = \frac{1}{2\pi\varepsilon_0} \sum_{k=1}^{N} \lambda_i \ \ell n(\left|\vec{r} - \vec{r}_i\right|), \quad \vec{r} \neq \vec{r}_i \tag{1.13}$$

$$\vec{E}(\vec{r}) = -\text{grad } V(\vec{r}) = \frac{1}{2\pi\varepsilon_0} \sum_{k=1}^{N} \frac{-\lambda_i}{(\left|\vec{r} - \vec{r}_i\right|)^2} (\vec{r} - \vec{r}_i) \tag{1.14}$$

The electrostatic force per unit length of wire i created by the rest of the system can be calculated as follows (wire i has a length L):

$$\vec{F}(\vec{r}_i) = \frac{1}{2\pi\varepsilon_0} \lambda_i \ \vec{E}(\vec{r}_i) = (\frac{1}{2\pi\varepsilon_0})^2 \ L \ \lambda_i \sum_{k=1}^{N} \frac{\lambda_k}{(\left|\vec{r}_i - \vec{r}_k\right|)^2} (\vec{r}_i - \vec{r}_k) \tag{1.15}$$

1.3. Analytic solution of the Laplace equation for geometries with wires and pads (no dielectric)

The following method is discussed by P.M. Morse and H. Feshbach [4].

1.3.1. The simplest problem is a **single wire and a conducting plane** (pad plane):

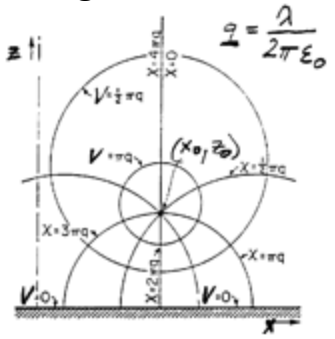

Fig.2 - Single wire and a pad plane.

We assume that the y axis is parallel to the direction of the wires, zero potential of the conducting plane (z = 0), and charge per unit of length λ. The solution of the Laplace equation is a complex potential F (in MKS units):

$$F(Y = x + iz) = V + i\chi = -\frac{\lambda}{2\pi\varepsilon_0} \ \ell n \frac{(Y - Y^0)}{(Y - \overline{Y}^0)} \tag{1.16}$$

where $Y = x + iz$ is a coordinate of a general point, $Y^0 = x_0 + iz_0$ is the position of the wire, $\overline{Y}^0 = x_0 - iz_0$ is the complex conjugate of Y^0. The real potential:

$$V(x,z) = \text{Re } F(Y) = -\frac{\lambda}{2\pi\varepsilon_0} \ \ell n \left[\frac{(x - x_0)^2 + (z - z_0)^2}{(x - x_0)^2 + (z + z_0)^2}\right] \tag{1.17}$$

1.3.2. We can expand the problem to a **system of many wires** located above the conducting plane using the superposition principle - see Fig. 3:

$$F(Y = x + iz) = -\frac{\lambda}{2\pi\varepsilon_0} \sum_{k=-\infty}^{k=+\infty} \ell n \frac{(Y - Y_k^0)}{(Y - \overline{Y}_k^0)} \qquad (1.18)$$

where Y_k^0 is the coordinate of the k-th wire. If all wires of the grid are spaced with uniform pitch s then one can write:

$$Y_k^0 = x_0 + ks + iz_0, \quad (k = \ldots -2, -3, 0, 1, 2, \ldots) \qquad (1.19)$$

where x_0 and z_0 are the wire coordinates for k = 0. The complex potential can then be written as a sum, which can be solved:

$$F(Y = x + iz) = -\frac{\lambda}{2\pi\varepsilon_0} \sum_{k=-\infty}^{k=+\infty} \ell n \frac{(Y - Y^0 - ks)}{(Y - \overline{Y}^0 - ks)} = -\frac{\lambda}{2\pi\varepsilon_0} \ell n \frac{\sin[(\pi / s)(Y - Y^0)]}{\sin[(\pi / s)(Y - \overline{Y}^0)]} \qquad (1.20)$$

and the corresponding real potential:

$$V(x,z) = \mathrm{Re}\ F(Y) = -\frac{\lambda}{2\pi\varepsilon_0} \ell n \frac{\sin^2[(\pi / s)(x - x_0)] + \sinh^2[(\pi / s)(z - z_0)]}{\sin^2[(\pi / s)(x - x_0)] + \sinh^2[(\pi / s)(z + z_0)]} \qquad (1.21)$$

1.3.3. With similar superposition techniques one can then construct the potential distribution of **more complex electrode structures** [3,5] - see Fig. 4:

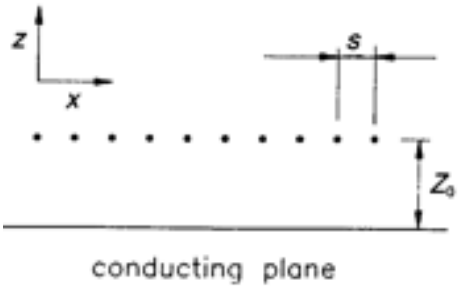

Fig.3 - Wire grid and a pad plane.

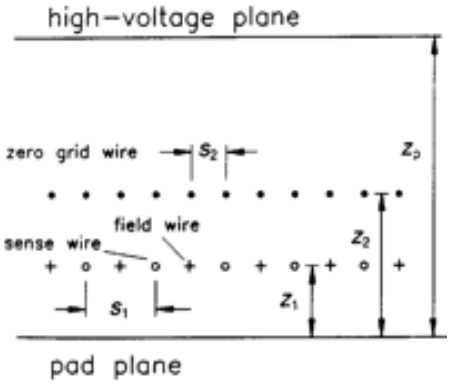

Fig.4 - A typical TPC geometry.

1.4. Numerical solution of Laplace equation for any shape of the electrodes (no dielectric)

A good reference is K.J. Binns and P.J. Lawrenson [6]; see also S. Yellin [7]. The numerical solution is based on the following steps: (a) conductor surfaces are specified by linking smooth curves,(b) create equally spaced lattice points with spacing d, (c) determine the topology of a given lattice point relative to the electrode structure; then assign an estimate of the potential per each lattice point, (d) the potential at each interior point of a group of four is average of its nearest neighbors - see Fig.5 for an example of CRID detector, (e) **iterate**; start first with a coarse lattice, then reduce it, etc.

We use the Gauss law in integral form. In absence of charges, the surface integral over the square in Fig. 5 is equal to zero:

$$\Phi = \oint_S \vec{E} \bullet d\vec{S} = \frac{1}{\varepsilon_0} \sum_i Q_i = 0 \qquad (1.22)$$

The electric filed in the n-th iteration is calculated on each surface boundary, for example $E_x^n = (V_{i-1,j}^n - V_{i,j}^n)/d$, etc. - see Fig. 5. By a simple algebra one obtains a simple equation used in the computation:

$$V_{i,j}^{n+1} = \frac{1}{4}[V_{i-1,j}^n + V_{i+1,j}^n + V_{i,j-1}^n + V_{i,j+1}^n] \qquad (1.23)$$

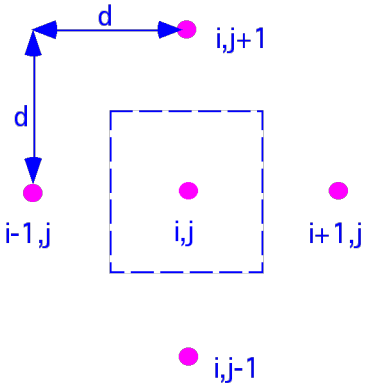

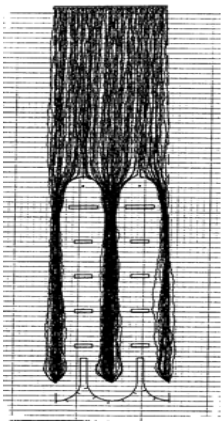

Fig.5 - Grid used to calculate potential distribution.

Fig.6 - Barrel CRID single electron detector.

1.5. Numerical solution of the Laplace equation for geometries with wires, pads and dielectric

We can follow the same procedure outlined in the previous problem [6]. However, we have to be more careful to account for the presence of charges within a given grid cubical of Fig.5. Again, we use the Gauss law in integral form:

$$\Phi = \oint_S \vec{E} \bullet d\vec{S} = \frac{1}{\varepsilon_r \varepsilon_0} \sum_i Q_i = \frac{1}{\varepsilon_r \varepsilon_0} (Q_{volume} + Q_{surface} + Q_{leakage} + Q_{ionization}) \qquad (1.24)$$

The potential in the center of cubical of Fig.5 is now calculated taking into account the charges within the cubical:

$$V_{i,j}^{n+1} = \frac{1}{4}[V_{i-1,j}^n + V_{i+1,j}^n + V_{i,j-1}^n + V_{i,j+1}^n + \frac{1}{\varepsilon_r \varepsilon_0} d^2 \sum_i Q_i] \qquad (1.25)$$

Example of a practical application of this method can be found in Ref. 8. For an alternative method of solution see Ref. 9.

Chapter 2

2. Electrostatic stability of a large system of wires

Equation describing the wire stability can be written as follows:

$$T\frac{d^2y}{dx^2} + F_{electrostatic} + F_{gravity} = 0 \qquad (2.1)$$

where T is mechanical tension on the wire per unit length, x is the coordinate along wire direction, y(x) is the displacement perpendicular to wire, $T\,d^2y/dx^2$ is restoring force per unit length, $F_{electrostatic}$ is electrostatic force per unit length and $F_{gravity}$ is gravitational force per unit length.

2.1. Solution A:

$F_{gravity}$ represents a constant force per unit length. This is not generally true for the electrostatic force $F_{electrostatic}$, which generally depends on a value of the displacement y(x). We are going to solve this problem **iteratively** assuming that in each step the electrostatic force is constant force per unit length just like the gravitational force (in the solution B this will not be assumed).

a) **Gravitational force on a wire** i**:**

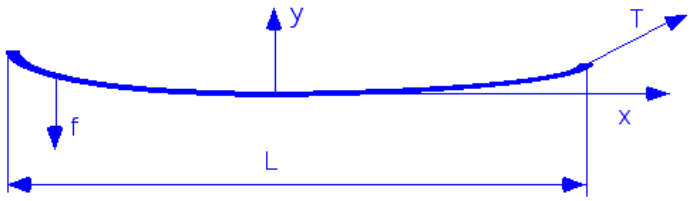

For the gravitational force alone, the solution of equation (2.1) is a parabola:

$$y(x) = \frac{f\,x^2}{2\,T} \qquad (2.2)$$

A wire sagitta at x = L/2 is: $s_g = y(x = \frac{L}{2}) = \frac{F_{gravity}\,L^2}{8\,T} = \frac{F_{TOT}\,L}{8\,T}$, (2.3)

where L is length of the wire, $F_{gravity}$ is force per unit length, F_{TOT} is a total force ($F_{gravity}$ L) and T is mechanical tension. In a large system of wires, the gravitational force on wire i is (i=1,...N):

$$F_{TOT}(\vec{r}_i) = L\,r_i\,p\,R_i^2\,g\,, \qquad (2.4)$$

where ρ_i is wire density, R_i is wire radii, L is length of the wire, g is gravitation constant.

Example of gravitational deflections:

Material	ρ [g/cm^3]	r [μm]	L [cm]		s [μm]	
W	19.3	10	6.063×10^{-5}	240	72	60
Cu-Be	8.23	50	6.464×10^{-4}	240	72	646
Al	2.7	50	2.121×10^{-4}	240	72	212
C	1.8	50	1.414×10^{-4}	240	72	141
s.s.	7.5	50	5.890×10^{-4}	240	72	589

b) **Electrostatic force created by the wire system:** see equation (1.15).

METHOD TO DETERMINE THE WIRE STABILITY [10]**:**
(a)Solve the 2-dimensional electrostatic problem for λ_i and determine the electrostatic and gravitational forces on each wire; (b) Include the 3-rd dimension by calculating the wire deflections $\vec{d}_i$ using the equation (2.3); (c) Move each wire by $\vec{d}_i$ in the 2-dimensional electrostatic problem and recalculate the electrostatic problem again and determine new λ_i; (d) Iterate in this way ~15 times. If the design is stable in 3-4 iteration, it is safe to build.

Does this simple minded approach work ?

Example #1 - 8-wire prototype for the OPAL central drift chamber [10]:

Anode wires **:** T = 101 g, 25 μm dia. W(Re),

Cathode wires **:** T = 620 g, 100 μm dia. Cu-Be

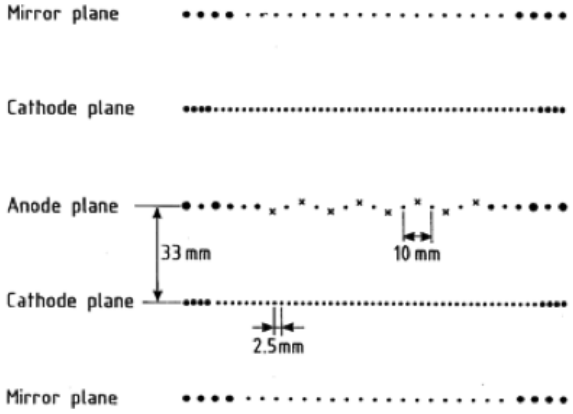

Fig.1 - Geometry of 4.5 m long drift cell; six wires (diameters 300, 175, 300, 175, 100 and 175 μm) terminate the anode plane at each side of the cell.

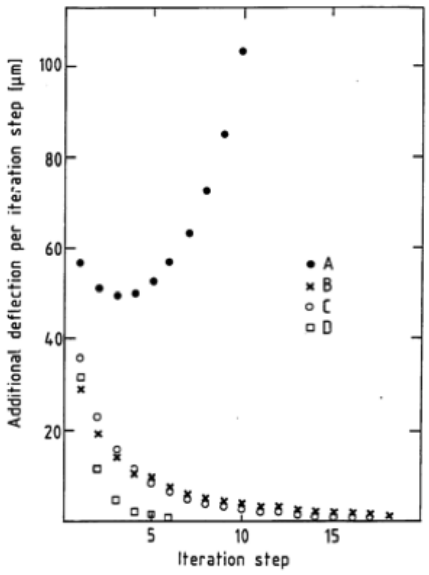

Fig.2 - Additional deflection as obtained in each iteration step of the iterative electrostatic calculation: (A) NiCoTi wire, 35 μm dia., length 4 m, T = 0.9 N, (B) NiCoTi wire, 35 μm dia.,

length 4 m, T = 1.2 N, (C) NiCoTi wire, 30 μm dia., length 4 m, T = 0.9 N, (D) W(Re) wire, 25 μm dia., length 4.5 m, T = 1.0 N.

Without the iterative electrostatic program, this prototype would have never worked. It is very difficult to guess stability of a 4.5 m long chamber like this. As a result of this study, the OPAL chamber was shortened from 4.5 m length to less than 4 m, and the NiCoTi wire was eliminated.

Example #2 - early study for the Mark II vertex chamber at SLC [11]:

Anode (T = 60 g, 20 μm dia. W), **Cathode**(T = 500 g, 150 μm dia. Cu-Be):

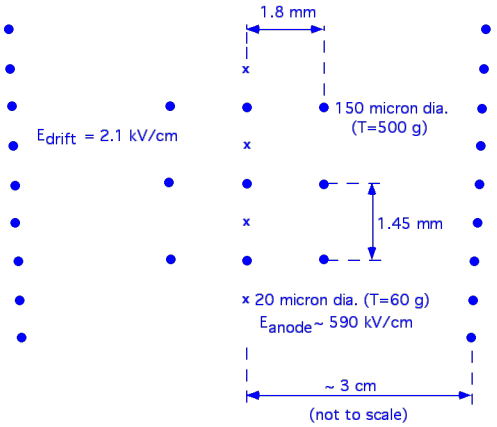

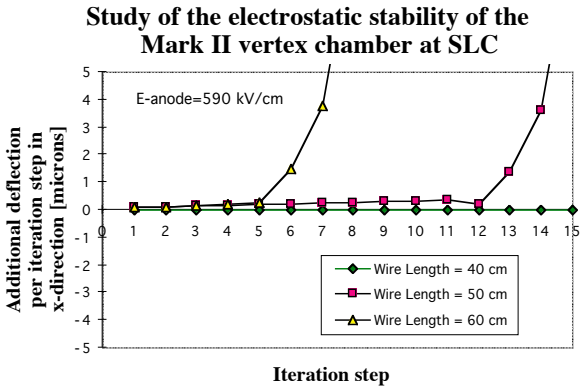

Example #3 - early study for the BaBar drift chamber at PEP II [12]:

Length: 2.5 m & 5 m

Anode: (T = 50 g, 20 μm dia. W), **Cathode:** (T = 25 & 50 g, 55 μm dia. Al):

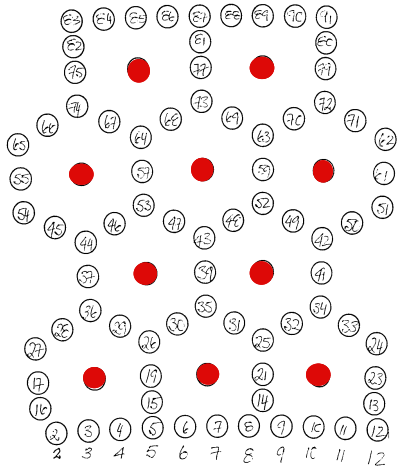

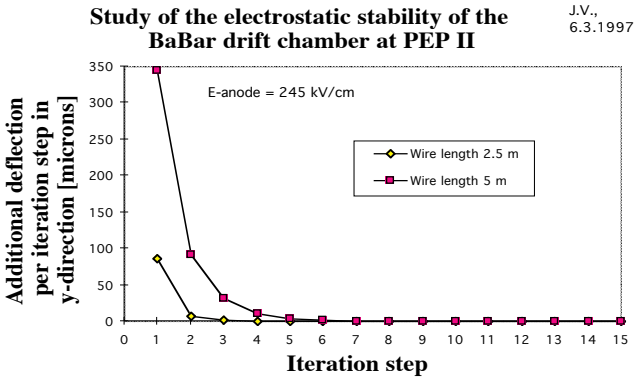

Notes:

(a) Vertex chambers with small wire spacing have similar severe electrostatic instability problems as very long chambers; (b) Ideal drift cells are symmetric such as BaBar drift cell; (c) A typical drift chambers design, such as the jet chamber, stagger the sense wires by some offset d to solve the left-right ambiguity. This will uniquely define a direction the sense wires will move; (d) One always balances gravitational deflection among different wires in the drift structure; (e) One must stay bellow a certain critical tension for a given choice of wires. This must be tested for each wire choice; (f) The advantage of the numerical method to evaluate the electrostatic stability is that one can find sensitivity to errors in wire tension, wire position, etc.

2.2. Solution B:

We will try to solve the equation (2.1) differently. We will assume that $F_{electrostatic}$ is proportional to the wire displacement y(x):

$$F_{electrostatic} \sim k\, y(x) \qquad (2.5)$$

Combining equations (2.1), (2.3) and (2.5) we obtain:

$$T\frac{d^2y}{dx^2} + k\,y(x) + \frac{8\,T s_g}{L^2} = 0 \qquad (2.6)$$

which has a solution:

$$y(x) = \frac{8 s_g T}{L^2 k}\left(\frac{\cos\sqrt{\frac{k}{T}}\left(x - \frac{L}{2}\right)}{\cos\sqrt{\frac{k}{T}}\frac{L}{2}} - 1\right) \qquad (2.7)$$

where s_g is the gravitational sagitta of the wire, T is mechanical tension on the wire per unit length, L is length of the wire and k is proportionality constant (do not know yet).

For x = L / 2 we get:

$$y\left(\frac{L}{2}\right) = \frac{8 s_g T}{L^2 k}\left(\frac{1}{\cos\sqrt{\frac{k}{T}}\frac{L}{2}} - 1\right) = \frac{2 s_g}{\chi^2}\left(\frac{1}{\cos\chi} - 1\right) \qquad (2.8)$$

One can see that the wire displacement diverges when $\chi = \sqrt{k/T}\,L/2 \sim \pi / 2$, i.e. the chamber becomes unstable. What is the constant k ? It can be shown that:

$$F_{electrostatic} = \frac{V^2}{2}\frac{dC}{dy} = \frac{V^2}{2}\left\{4\pi\varepsilon_0 \frac{1}{[a\ \ell n(a / r)]^2}\right\} y(x) = k\, y(x) \qquad (2.9)$$

where dC/dy is change in capacitance per unit length due to displacement in y, V is potential of the wire, r is wire radius, a is typical distance of the wire to the other electrodes. From equation (2.9) we now understand why vertex chambers with small wire spacing have electrostatic problems. As the wire spacing gets small the inter-electrode capacitance gets larger, and therefore we need larger voltages to get the same wire charge. The instability is

proportional to voltage square. The wires may also start vibrating in a presence of large radiation [13], and one has to consider the wire friction of gas in equation (2.1).

Chapter 3:

3.1. Drift of electrons and ions in gases (macroscopic view)

A single electron moving in electric and magnetic fields, $\vec{E}$ and $\vec{B}$, and under the influence of a **frictional force,** can be described by a system of linear differential equations:

$$m\frac{d\vec{v}}{dt} = e\vec{E} + e[\vec{v}\,x\,\vec{B}] - K\vec{v} \qquad (3.1)$$

where m - is the mass of the electron, e - is the electric charge of a particle, $\vec{v}$ - is drift velocity vector, $K\vec{v}$ - "Langevin" frictional force, K is a constant, m/K - has a dimension of time (will call it the characteristic time $\tau \equiv$ m/K).

We are interested in a steady state solution of equation (1), $d\vec{v}/dt = 0$, which occurs for $t >> \tau$. From the equation (3.1) we get :

$$\frac{d\vec{v}}{dt} = 0 = \frac{e}{m}\vec{E} + \frac{e}{m}[\vec{v}\,x\,\vec{B}] - \frac{K}{m}\vec{v},$$

$$\frac{e}{m}\vec{E} = \frac{K}{m}\vec{v} - \frac{e}{m}[\vec{v}\,x\,\vec{B}],\ \frac{e}{m}\vec{E} = \frac{1}{\tau}\vec{v} - \frac{e}{m}[\vec{v}\,x\,\vec{B}] \qquad (3.2)$$

Let's define the new variables (ω is the cyclotron frequency):

$$\vec{\omega} = \frac{e}{m}\vec{B},\vec{\varepsilon} = \frac{e}{m}\vec{E},\ \mu = \frac{e}{m}\tau \qquad (3.3)$$

Equation (3.2) changes to:

$$\vec{\varepsilon} = \frac{1}{\tau}\vec{v} - [\vec{v}\,x\,\vec{\omega}] \qquad (3.4)$$

where

$$\vec{v}\,x\,\vec{\omega} = \begin{pmatrix} i & j & k \\ v_x & v_y & v_z \\ \omega_x & \omega_y & \omega_z \end{pmatrix} \qquad (3.5)$$

Expressing equations (3.4) and (3.5) explicitly:

$$\varepsilon_x = \frac{1}{\tau}v_x - \omega_z v_y + \omega_y v_z,\ \varepsilon_y = \omega_z v_x + \frac{1}{\tau}v_y - \omega_x v_z,\ \varepsilon_z = -\omega_y v_x + \omega_x v_y + \frac{1}{\tau}v_z \qquad (3.6)$$

This can be rewritten in a matrix form:

$$M\,\vec{v} = \vec{\varepsilon} \qquad (3.7)$$

where

$$M = \begin{pmatrix} \frac{1}{\tau} & -\omega_z & \omega_y \\ \omega_z & \frac{1}{\tau} & -\omega_x \\ -\omega_y & \omega_x & \frac{1}{\tau} \end{pmatrix} \qquad (3.8)$$

The solution is obtained by inverting matrix M: (3.10)

$$\vec{v} = M^{-1}\,\vec{\varepsilon} \tag{3.9}$$

$$M^{-1} = \frac{\tau}{1+\omega^2\tau^2}\begin{pmatrix} 1+\omega_x^2\tau^2 & \omega_z\tau+\omega_x\omega_y\tau^2 & -\omega_y\tau+\omega_x\omega_z\tau^2 \\ -\omega_z\tau+\omega_x\omega_y\tau^2 & 1+\omega_y^2\tau^2 & \omega_x\tau+\omega_y\omega_z\tau^2 \\ \omega_y\tau+\omega_x\omega_z\tau^2 & -\omega_x\tau+\omega_y\omega_z\tau^2 & 1+\omega_z^2\tau^2 \end{pmatrix}$$

where $$\omega^2 = \omega_x^2 + \omega_y^2 + \omega_z^2 = \left(\frac{e}{m}\right)^2 B^2 \tag{3.11}$$

is the square of the cyclotron frequency of the electron.

The final solution can be rewritten after some algebra in a form:

$$\vec{v} = \frac{\mu}{1+(\omega\tau)^2}\left[\vec{E} + \frac{\omega\tau}{B}[\vec{E}\times\vec{B}] + (\omega\tau)^2\frac{\vec{E}\cdot\vec{B}}{B^2}\vec{B}\right] \tag{3.12}$$

where the drift direction is governed by the dimensionless parameter $\omega\tau$. For $\omega\tau = 0$, $\vec{v}$ is parallel to $\vec{E}$, and equation (3.12) yields: $\vec{v} = \mu\vec{E}$, where μ is the electron mobility, which is proportional to the characteristic time between collisions . From equation (3.11) we obtain $\omega\tau = e/m\,B\,\tau$.

For $\omega\tau = 0$ ==> $\vec{v} = \mu\vec{E}$, i.e. $\vec{v}$ is aligned with $\vec{E}$,

$\omega\tau$ large ==> $\vec{v}$ tends to be aligned along $\vec{B}$,

$\omega\tau$ large & $\vec{E}.\vec{B} = 0$ ==> $\vec{v}$ tends to be aligned along $\vec{E}\times\vec{B}$.

In practical chambers we have these conditions typically: $\mu \sim 10^4$ cm^2 V^{-1} s^{-1} for electrons, $\mu \sim 1$ cm^2 V^{-1} s^{-1} for ions, $B \le 1$ T $= 10^{-4}$ V s cm^{-2}, $\omega\tau = B\mu \approx 10^{-4}$ for ions, $\omega\tau = B\mu \approx 1$ for electrons, $\tau \approx$ 2-5 psec for electrons, $1/\tau \approx$ (2-5) x 10^{11} Hz collision rate for electrons. The effect of typical magnetic fields on ion drift is negligible.

Example #1 - $\vec{E}$ is perpendicular to $\vec{B}$, i.e. $\vec{E}.\vec{B}=0$, $\vec{E} = (E_x,0,0)$, $\vec{B} = (0,0,B_z)$:

From equation (3.12) we obtain:

$$v_x = \frac{\mu}{1+(\omega\tau)^2}E_x \equiv \frac{\mu}{1+(\omega\tau)^2}\left|\vec{E}\right|,\ v_y = -\frac{\mu}{1+(\omega\tau)^2}\frac{\omega\tau}{B_z}E_x B_z \equiv -\frac{\mu}{1+(\omega\tau)^2}\omega\tau\left|\vec{E}\right|,$$

$$v_z = 0 \tag{3.13}$$

Lorentz angle θ_{xy}: $$\tan\theta_{xy} = \frac{v_y}{v_x} = -\omega\tau \tag{3.14}$$

By measuring the Lorentz angle we determine $\omega\tau$. The drift velocity magnitude:

$$v(E,B) = \sqrt{v_x^2 + v_y^2} = \frac{\mu}{\sqrt{1+(\omega\tau)^2}}\left|\vec{E}\right| = \mu\left|\vec{E}\right|\cos\theta_{xy} =$$

$$= v(E,B=0)\cos\theta_{xy} = v(E\cos\theta_{xy},B=0) \tag{3.15}$$

This is known as **Tonk's theorem** [14]. Experimental verification of the Tonk's theorem for methane c an be found in Ref. 15.

Example #2 - $\vec{E}$ is parallel to $\vec{B}$, i.e. $\vec{E} \times \vec{B} = 0$, $\vec{E} = (0,0,E_z)$, $\vec{B} = (0,0,B_z)$

From equation (3.12) we obtain:

$$v_x = 0,\ v_y = 0,\ v_z = \frac{\mu}{1+(\omega\tau)^2}\ [E_z + (\omega\tau)^2 \frac{E_z \cdot B_z}{B^2} B_z] \equiv \mu \left|\vec{E}\right| \qquad (3.16)$$

Example #3 - $\vec{E}$ is nearly parallel to $\vec{B}$, i.e. $\left|\vec{B}\right| \approx B_z$, $\vec{E} = (0,0,E_z)$, $\vec{B} = (0,B_y,B_z)$, $B_y << B_z$:

First we evaluate: $\vec{E}.\vec{B} = E_x B_x + E_y B_y + E_z B_z = E_z B_z$

$$\vec{E} \times \vec{B} = \begin{pmatrix} i & j & k \\ E_x & E_y & E_z \\ B_x & B_y & B_z \end{pmatrix} = \begin{pmatrix} i & j & k \\ 0 & 0 & E_z \\ 0 & B_y & B_z \end{pmatrix} = i\, E_z\, B_y$$

From equation (3.12) we obtain:

$$v_x = \frac{\mu}{1+(\omega\tau)^2}\ \frac{\omega\tau}{B} E_z\, B_y \approx \frac{\omega\tau}{1+(\omega\tau)^2}\ \frac{B_y}{B_z}\ v(B=0)$$

$$v_y = \frac{\mu}{1+(\omega\tau)^2}\ (\omega\tau)^2\ \frac{E_z \cdot B_z}{B^2} B_y \approx \frac{(\omega\tau)^2}{1+(\omega\tau)^2}\ \frac{B_y}{B_z}\ v(B=0) \qquad (3.17)$$

$$v_z = \frac{\mu}{1+(\omega\tau)^2} [E_z + (\omega\tau)^2 \frac{E_z \cdot B_z}{B^2} B_z] \approx \mu\, E_z = v(B=0)$$

where $v(B=0) = \mu\, E_z$ is drift velocity for $B = 0$. We can define two Lorentz angles:

$$\tan\theta_{yz} = \frac{v_y}{v_z} = \frac{(\omega\tau)^2}{1+(\omega\tau)^2}\ \frac{B_y}{B_z},\ \tan\theta_{xy} = \frac{v_y}{v_x} = \omega\tau \qquad (3.18)$$

SLD CRID example:

(a) $B_z(r,z) = B_z^0 + \frac{1}{2} B_r^0\ \frac{r^2 - 2z^2}{r_0 z_0}$, $B_z^0 = 0.6$ T, $B_r(r,z) = B_r^0\ \frac{r\ z}{r_0\ z_0} = \kappa\ z$, $r_0 = 1.2$ m, $z_0 = 1.5$ m, $B_r^0 = 0.0214$ T, (b) assume that B_r is parallel with y axis ($B_r \approx B_y$), (c) electric field E ~ 400 V/cm, (d) drift velocity of 4.3 cm/μs, (e) $\omega\tau \sim 0.87$ and $\theta_{xy} \sim 41^o$ for C_2H_6 gas [16], (f) TPC active length is between $z_1 = 0.1$ m and $z_2 = 1.2$ m.

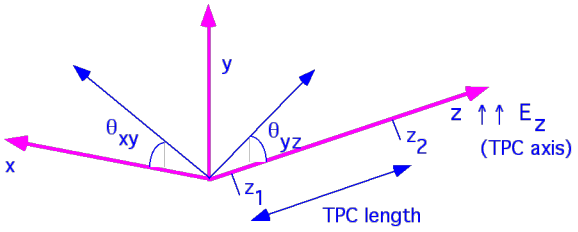

Expected distortion in x-direction:

$$\delta_x = \int_{t_1}^{t_2} v_x \, dt \approx \frac{\omega\tau}{1+(\omega\tau)^2} \frac{v(B=0)}{B_z} \int_{t_1}^{t_2} B_r \, dt =$$

$$= \frac{\omega\tau}{1+(\omega\tau)^2} \frac{1}{B_z} \int_{z_1}^{z_2} B_r \, dz = \frac{\omega\tau}{1+(\omega\tau)^2} \kappa [z_2^2 - z_1^2] \approx 9.9 \text{ mm} \qquad (3.19)$$

where κ is a constant: $\kappa = \frac{1}{2} \frac{B_r^0}{B_z} \frac{r}{r_0 z_0}$.

Similarly for y-direction:

$$\delta_y = \int_{t_1}^{t_2} v_y \, dt \approx \frac{(\omega\tau)^2}{1+(\omega\tau)^2} \frac{v(B=0)}{B_z} \int_{t_1}^{t_2} B_r \, dt =$$

$$= \frac{(\omega\tau)^2}{1+(\omega\tau)^2} \frac{1}{B_z} \int_{z_1}^{z_2} B_r \, dz = \frac{(\omega\tau)^2}{1+(\omega\tau)^2} \kappa [z_2^2 - z_1^2] \approx 8.6 \text{ mm} \qquad (3.20)$$

These calculations were verified by the measurement using the UV fiducial fibers [17].

3.2. The drift of electrons in gases (simple microscopic view)

The simple macroscopic theory, based on a concept of the friction force, cannot predict $\omega\tau$, which has to be obtained by measuring the Lorentz angle. Can we do better by introducing the following details of the electron-molecule collisions ?

1) As electron moves in the gas it suffers random collisions with molecules of the gas. We assume that there is no correlation in the direction before and after the collision.

2) Number of collisions n in drift distance x is related to the average drift velocity v as follows: $n = (x / v)(1 / \tau)$ (3.21)

where τ is an average time between collisions and $1/\tau$ - is average rate of collisions.

3) The average time between collisions τ is related to the electron instantaneous velocity V_{inst}, the collision cross-section σ and the density of the gas N as follows:

$$1 / \tau = N \sigma v_{inst} \qquad (3.22)$$

3) We will introduce the differential probability P of having the next collision between time t and t + dt: $P = 1/\tau \, e^{-t/\tau} \, dt$ (3.23)

We will show that this "new picture" will confirm results obtained using the

macroscopic concept of the friction force. However, as we will see, this new picture is still too simplistic.

Example #1 - a uniform electric field E and no magnetic field:

An electron between collisions moves accordingly to the equation of motion:

$$m \frac{dv}{dt} = e E \tag{3.24}$$

Its solution is the electron displacement as a function of time is $x(t) = \frac{1}{2} \frac{e}{m} E t^2$.

The average displacement $< x >$ at average time between collisions τ is obtained by averaging x(t) over time t, using the probability distribution of t, i.e. equation (3.23):

$$< x > = \int_0^\infty \frac{1}{2} \frac{e}{m} E t^2 \frac{1}{\tau} e^{-t/\tau} dt = \frac{e}{m} E \tau^2 \tag{3.25}$$

The average electron drift velocity is defined as:

$$< v > = \frac{< x >}{\tau} = \frac{e}{m} E \tau = \mu E \tag{3.26}$$

Example #2 - $\vec{E}$ is perpendicular to $\vec{B}$, i.e. $\vec{E}.\vec{B}=0$, $\vec{E} = (E_x, 0, 0)$, $\vec{B} = (0, 0, B_z)$:

An electron between collisions moves accordingly to the equation of motion:

$$m \frac{d\vec{v}}{dt} = e \vec{E} + e [\vec{v} \times \vec{B}] \tag{3.27}$$

which can be rewritten as a system of differential equations:

$$m \frac{dv_x(t)}{dt} = e E_x + e v_y B_z, \; m \frac{dv_y(t)}{dt} = -e v_x B_z, \; m \frac{dv_z(t)}{dt} = 0 \tag{3.28}$$

We introduce the cyclotron frequency $\omega = e/m B_z$ and obtain the solution for the initial conditions $v_x(0) = v_y(0) = v_z(0) = 0$:

$$v_x(t) = (\frac{e}{m} E_x \frac{1}{\omega}) \sin \omega t \, , \; v_y(t) = (\frac{e}{m} E_x \frac{1}{\omega}) (\cos \omega t - 1) \, , \; v_z(t) = 0 \tag{3.29}$$

The drift velocity is then given by the following averages ($\mu = e/m \tau$):

$$< v_x(t) > = \frac{e}{m} E_x \frac{1}{\omega} \int_0^\infty \sin \omega t \frac{1}{\tau} e^{-t/\tau} dt = \frac{e}{m} \frac{E_x \tau}{1 + (\omega \tau)^2} = \frac{\mu}{1 + (\omega \tau)^2} E_x$$

$$< v_y(t) > = \frac{e}{m} E_x \frac{1}{\omega} \int_0^\infty (\cos \omega t - 1) \frac{1}{\tau} e^{-t/\tau} dt = -\frac{e}{m} \frac{E_x \omega \tau^2}{1 + (\omega \tau)^2} = \frac{\mu}{1 + (\omega \tau)^2} \frac{\omega \tau}{B_z} E_x B_z \tag{3.30}$$

$$< v_z(t) > = 0$$

We have obtained the same results as in equations (3.15) which was derived from the friction force model. The Lorentz angle θ_{xy} is:

$$\tan\theta_{xy} = \frac{v_y}{v_x} = -\omega\tau(E,B) \equiv -\frac{e}{m} B\tau = -\mu B = -\frac{v(E,B=0)\,B}{E} \qquad (3.31)$$

However, in practice the equation (3.31) is only approximate because our modeling of electron collisions with the gas is too simple minded. The correct equation is :

$$\tan\theta_{xy} = \psi\,\frac{v(E,B=0)\,B}{E} \qquad (3.32)$$

where $\psi = \psi(E/N, B/N)$ is the **magnetic deflection factor.**

Measurement of the magnetic deflection factor ψ was done by T. Kunst, B. Goetz and B. Schmidt [15] - see Fig. 1. The fact that it is not really a constant casts a doubt that we are dealing with a real theory so far.

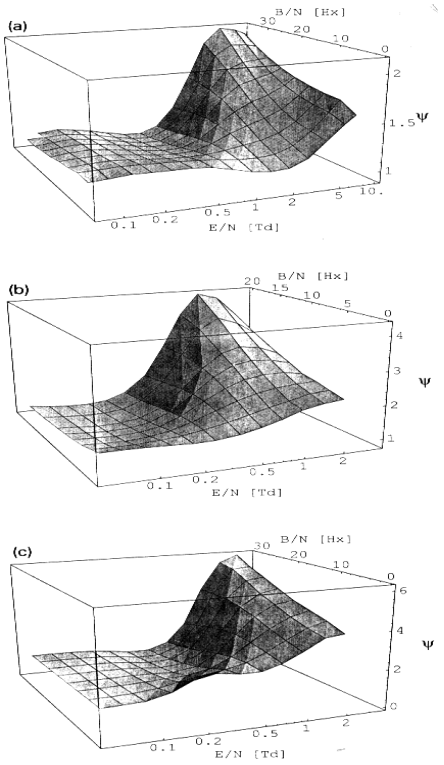

Fig. 1 - Magnetic deflection factor ψ for (a) CH_4, (b) 90% Ar+10% CH_4, (c) 95% Ar + 5% CH_4 gases.

Example #3: - $\vec{E}$ is nearly parallel to $\vec{B}$, i.e. $|\vec{B}| \approx B_z$, $\vec{E} = (0,0,E_z)$, $\vec{B} = (0,B_y,B_z)$, $B_y << B_z$:

From equation (3.27) we obtain a system of differential equations:

$$m\frac{dv_x(t)}{dt} = e(v_y B_z - v_z B_y),\ m\frac{dv_y(t)}{dt} = -e\ v_x B_z,\ m\frac{dv_z(t)}{dt} = e\ E_z + e\ v_x B_y \qquad (3.33)$$

The solution for the initial conditions $v_x(0) = v_y(0) = v_z(0) = 0$:

$$v_x(t) = \frac{B_y E_z}{B^2}(\cos\omega t - 1),\ v_y(t) = \frac{B_y B_z E_z}{B^3}(\omega t - \sin\omega t) \qquad (3.34)$$

$$v_z(t) = \frac{E_z}{B^3}(B_z^2\,\omega t + B_y^2 \sin\omega t)$$

The drift velocity is then given by the following averages:

$$< v_x(t) > = \frac{B_y E_z}{B^2}\int_0^\infty (\cos\omega t - 1)\frac{1}{\tau} e^{-t/\tau} dt = -\frac{\mu^2}{1+(\omega\tau)^2} B_y E_z \qquad (3.35)$$

$$< v_y(t) > = \frac{B_y B_z E_z}{B^3}\int_0^\infty (\omega t - \sin\omega t)\frac{1}{\tau} e^{-t/\tau} dt = \frac{\mu^3}{1+(\omega\tau)^2} B_y B_z E_z$$

$$< v_z(t) > = \frac{E_z}{B^3}\int_0^\infty (B_z^2\,\omega t + B_y^2 \sin\omega t)\frac{1}{\tau} e^{-t/\tau} dt = \frac{1+\mu^2 B_z^2}{1+(\omega\tau)^2}\mu E_z$$

We have obtained the same results as in equations (3.17). This supports our previous intuition that the characteristic time in the friction model is the same as the average time between collisions in the simple microscopic model. However, in all these examples, $\omega\tau$ and μ had to be obtained in the end from the experiment, and -not- from the theory !! Before we mention the real theory, we have to introduce a concept of electron diffusion.

3.3. Electron diffusion

Drifting electrons scatter on the gas molecules. Their motion can be described by their random motion, which is characterized by the mean energy ε and gives rise to diffusion, and by their collective motion, which is characterized by the average drift velocity. The motion follows the continuity equation (the total electron current is given by the sum of the drift current and the diffusion current: $\vec{J} = n\vec{v} - D\vec{\nabla}n$). Its solution has in the simplest case the isotropic distribution, i.e. the point-like cloud of electrons at time t = 0 will create a Gaussian density distribution at time t :

$$n = \left(\frac{1}{\sqrt{4\pi Dt}}\right)^3 \exp\left(-\frac{r^2}{4Dt}\right), \qquad (3.36)$$

where D is the **diffusion coefficient.** From equation (3.37) follows that the diffusion width of an electron cloud σ_x, after starting point-like and traveled time interval t, is:

$$\sigma_x = \sqrt{2Dt} \tag{3.37}$$

One can show that the diffusion coefficient is related to electron energy ε as follows:

$$D = \frac{2}{3}\frac{\varepsilon}{m}\tau = \frac{\varepsilon_k}{m}\tau \tag{3.38}$$

where ε is electron energy, ε_k is so called **"characteristic energy",** m is mass of the electron and τ is average time between collisions. Recalling the expression for electron mobility, we obtain expression for the characteristic electron energy:

$$\varepsilon_k = \frac{Dm}{\tau} = \frac{Dm}{\frac{\mu m}{e}} = \frac{De}{\mu}. \tag{3.39}$$

The diffusion width σ_x of an electron cloud width, after starting point-like and traveled over a distance x:

$$\sigma_x = \sqrt{2Dt} = \sqrt{\frac{2Dx}{\mu E}} = \sqrt{\frac{2\varepsilon_k x}{eE}}. \tag{3.40}$$

The smallest diffusion corresponds to a thermal energy $\varepsilon_k = kT$, ($\varepsilon = 3/2\ kT \sim 0.04$ eV at 24°C) resulting in the smallest possible diffusion width σ_x of an electron cloud (so called "**thermal limit**"):

$$\sigma_x = \sqrt{2Dt} = \sqrt{\frac{2kTx}{eE}}. \tag{3.41}$$

However the reality is unfortunately more complicated:

1. Electric field alters the diffusion so that it is necessary to introduce two diffusion coefficients D_L and D_T, one for the longitudinal and one transverse direction in respect to electric field. Fig. 2 shows an example in methane [18].

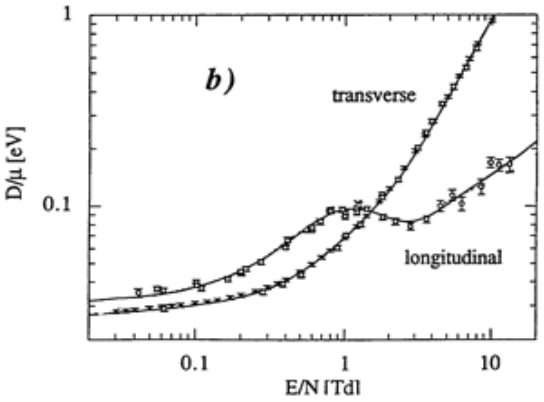

Fig.2 - Diffusion coefficient in methane.

2. Magnetic field alters the diffusion so that the transverse diffusion coefficient $D_T(B)$ in respect to its direction gets smaller:

$$\frac{D_T(B)}{D_T(B=0)} = \frac{1}{1+(\omega\tau)^2}, \tag{3.42}$$

while the longitudinal diffusion coefficient remains the same $D_L(B) = D_L(0)$.

3.4. Boltzmann equation method.

A full theory of electron transport in gases can get rather complicated. We will follow more simple path of Schultz and Gresser [19]. For more complete description see L. G. H. Huxley and R.W. Crompton [20]. For a theory which includes the ionization and attachment processes see K.F. Ness and R.E. Robson, [21].

Drifting electrons scatter on the gas molecules. This motion follows the Boltzmann transport equation, which expresses the conservation of number of electrons. If f(v,r,t) is the distribution function of electrons at r, v of the phase space at time t, the simplest 1-dimensional form of the Boltzmann equation is:

$$\frac{\partial f}{\partial t} + \frac{\partial f}{\partial r}\frac{\partial r}{\partial t} + \frac{\partial f}{\partial v}\frac{\partial v}{\partial t} - \left.\frac{\partial f}{\partial t}\right|_{Coll.} = 0 \qquad (3.43)$$

where $\partial f/\partial t$ represents time evolution of f(v,r,t), $(\partial f/\partial r)(\partial r/\partial t)$ represents loss of electrons in interval dr due to diffusion, $(\partial f/\partial v)(\partial v/\partial t)$ represents loss of electrons in interval dv due to acceleration caused by field E and $\partial f/\partial t|_{Coll.}$ represents loss of electrons in interval dv due to collisions of electrons with molecules of a gas.

To solve the equation (3.47) we introduce the following simplifications:

a) We express the distribution function f using electron energy $\varepsilon = 1/2 m v^2$, and the mean free path $\ell(\varepsilon)$ between two elastic collisions,

b) we assume that the electric field E is parallel with x axis (no magnetic field for now),

c) we assume a stationary case, i.e. no x or t dependence,

d) we assume **no ionization and no attachment processes**,

e) we expand the distribution function f in terms of the Legendre polynomial expansion, and use in our case **two terms only**:

$$f = f_0(\varepsilon) + f_1(\varepsilon)\cos\theta + \ldots \qquad (3.44)$$

One gets two coupled equations :

$$eE\frac{\partial f_0}{\partial v} + mv\frac{\partial f}{\partial x} = -\frac{m v f_1}{\ell(\varepsilon)}, \quad \frac{eE}{2v}\frac{\partial}{\partial v}(v^2 f_1) + \frac{1}{2}mv^2\frac{\partial f_1}{\partial x} = \frac{m^2}{M}\frac{3}{2v}\frac{\partial}{\partial v}\left(\frac{v^4 f_0}{\ell(\varepsilon)}\right) \qquad (3.45)$$

where M is mass of the molecule.

We now assume $\partial f/\partial x = 0$, i.e. uniform distribution along x direction. This yields these two equations:

$$eE\frac{\partial f_0}{\partial v} = -\frac{m v f_1}{\ell(\varepsilon)}, \quad \frac{eE}{2v}\frac{\partial}{\partial v}(v^2 f_1) = \frac{m^2}{M}\frac{3}{2v}\frac{\partial}{\partial v}\left(\frac{v^4 f_0}{\ell(\varepsilon)}\right) \qquad (3.46)$$

One can now eliminate f_1 and solve for f_0 :

$$\frac{2}{3}\frac{(eE)^2}{m}\frac{\partial}{\partial\varepsilon}[\varepsilon\ell(\varepsilon)\frac{\partial(f_0/v)}{\partial\varepsilon}]+\frac{2m}{M}\frac{\partial}{\partial\varepsilon}[\frac{\varepsilon v f_0}{\ell(\varepsilon)}]=0 \qquad (3.47)$$

Equation (3.47) can be easily solved (first, we assume $\ell(\varepsilon)$ = const.) :

$$f_0(\varepsilon)=C\sqrt{\varepsilon}\ \exp[-\frac{3m}{M}(\frac{\varepsilon}{eE\ell(\varepsilon)})^2] \qquad (3.48)$$

where a constant C is obtained from a normalization : $\int_0^{\varepsilon_{max}} f_0(\varepsilon)d\varepsilon=1$. A fraction of energy lost by electron scattering elastically from molecule of mass M can be approximated as:

$$\frac{\Delta\varepsilon}{\varepsilon}=\frac{2m}{M}(1-\cos\theta), \qquad (3.49)$$

while the mean fraction of energy lost is $\Lambda=2m/M$. However, the solution (3.48) must be changed if $\ell(\varepsilon)$ is not a constant and if the mean fraction of energy lost in the collision is not equal to $\Lambda=2m/M$, but it is $\Lambda=\Lambda(\varepsilon)$. In this case equation (3.48) becomes :

$$f_0(\varepsilon)=C\sqrt{\varepsilon}\ \exp[-\int_0^{\varepsilon}\frac{3\Lambda(\varepsilon')\varepsilon'}{(eE\ell(\varepsilon'))^2}d\varepsilon'] \qquad (3.50)$$

Unfortunately, one has to introduce several complications:

a) If the energy of electrons is similar as the thermal energy of the molecules (ε = kT ~ 0.025 eV), it is necessary to introduce an additional term in equation (3.47):

$$\frac{2}{3}\frac{(eE)^2}{m}\frac{\partial}{\partial\varepsilon}[\varepsilon\ell(\varepsilon)\frac{\partial(f_0/v)}{\partial\varepsilon}]+\frac{2m}{M}\frac{\partial}{\partial\varepsilon}[\frac{\varepsilon v f_0}{\ell(\varepsilon)}]+\frac{\partial}{\partial\varepsilon}[\frac{2\Lambda(\varepsilon)}{m}]\frac{\varepsilon^2}{\ell(\varepsilon)}\,kT\frac{\partial(f_0/v)}{\partial\varepsilon}=0 \qquad (3.51)$$

This changes solution (3.50) to:

$$f_0(\varepsilon)=C\sqrt{\varepsilon}\ \exp[-\int_0^{\varepsilon}\frac{3\Lambda(\varepsilon')\varepsilon'}{[(eE\ell(\varepsilon'))^2+3\Lambda(\varepsilon')\varepsilon'kT]}d\varepsilon'] \qquad (3.52)$$

b) If we wish to add inelastic collisions, we must add to equation (3.51) additional term:

$$\sum_k[\frac{\sqrt{2/m}\sqrt{(\varepsilon+\varepsilon_k)}}{\ell_k(\varepsilon+\varepsilon_k)}f_0(\varepsilon+\varepsilon_k)-\frac{\sqrt{2/m}\sqrt{\varepsilon}}{\ell_k(\varepsilon)}f_0(\varepsilon)], \qquad (3.53)$$

where ε_k is the excitation energy of the k-th state and ℓ_k is the mean free path between two collisions which gives rise to the excitation. In practice, the inelastic collisions are vibrational and rotational molecular excitations caused by electrons of sufficient energy. We can approximate equation (3.53) by :

$$\sum_k \varepsilon_k\frac{\partial}{\partial\varepsilon}[\frac{v f_0(\varepsilon)}{\ell_k(\varepsilon)}] \qquad (3.54)$$

and the solution (3.50) is still valid provided we use :

$$\Lambda(\varepsilon)=\frac{2m}{M}+\sum_k\frac{\varepsilon_k}{\varepsilon}\frac{\ell_e(\varepsilon)}{\ell_k(\varepsilon)} \qquad (3.55)$$

The last equation can be expressed in terms of cross sections :

$$\Lambda(\varepsilon) = \frac{2m}{M} + \sum_k \frac{\varepsilon_k}{\varepsilon} \frac{\sigma_k(\varepsilon)}{\sigma_e(\varepsilon)} \tag{3.56}$$

where $\sigma(\varepsilon) = 1/N\ell(\varepsilon)$ is the cross section, $N=N_0$ (p/760) (273/T) is the Loschmidt number, N_0 is the Loschmidt number defined at 0°C (2.687 x 10^{25} molecules/m^3), p is pressure in Torr and T is absolute temperature in K.

c) Finally, one includes magnetic field. This results in the following modification of the solution (3.50) ($\vec{E}$ is perpendicular to $\vec{B}$):

$$f_0(\varepsilon) = C\sqrt{\varepsilon}\ \exp\left[-\int_0^{\varepsilon} \frac{3\Lambda(\varepsilon')G(B)\varepsilon'}{[(eE\ell(\varepsilon'))^2 + 3\Lambda(\varepsilon')\varepsilon' kT\, G(B)]} d\varepsilon'\right] \tag{3.57}$$

where

$$G(B) = 1 + \frac{e^2 B_z^2 \ell_e(\varepsilon)^2}{2m\varepsilon} \tag{3.58}$$

d) Gas mixtures are calculated as follows:

$$\sigma = \sum_i \delta_i \sigma^i,\ \sigma\Lambda = \sum_i \delta_i \sigma^i \Lambda_i \tag{3.59}$$

Once we obtain the function $f_0(\varepsilon)$, the electron transport coefficients are calculated as follows ($\vec{E}$ is perpendicular to $\vec{B}$):

1. Drift velocity :

$$v_x = -\frac{2}{3}\frac{eE}{m}\int_0^{\varepsilon_{max}} \frac{\varepsilon \ell_e(\varepsilon)}{G(B)} \frac{\partial(f_0(\varepsilon)/\nu(\varepsilon))}{\partial\varepsilon} d\varepsilon,\ v_y = \frac{eEeB}{3m}\int_0^{\varepsilon_{max}} \frac{\ell_e^2(\varepsilon)\nu(\varepsilon)}{G(B)} \frac{\partial(f_0(\varepsilon)/\nu(\varepsilon))}{\partial\varepsilon} d\varepsilon$$

$$v = \sqrt{v_x^2 + v_y^2} \tag{3.60}$$

2. Lorentz angle : $$\theta = \tan^{-1}\left(\frac{v_y}{v_x}\right) \tag{3.61}$$

3. The diffusion coefficient : $$D_T = \frac{1}{3}\int_0^{\varepsilon_{max}} \frac{\ell_e(\varepsilon)\nu(\varepsilon)}{G(B)} f_0(\varepsilon) d\varepsilon \tag{3.62}$$

From the Lorentz angle we determine the $\omega\tau$ term needed in many equation in the earlier part of the lecture. The theory works with a 5-10% accuracy. The following three examples were calculated by the author using a code written by P. Coyle following the Schultz and Gresser theory [22]:

<u>Example #1</u> ($f_0(\varepsilon)$ function in methane) :

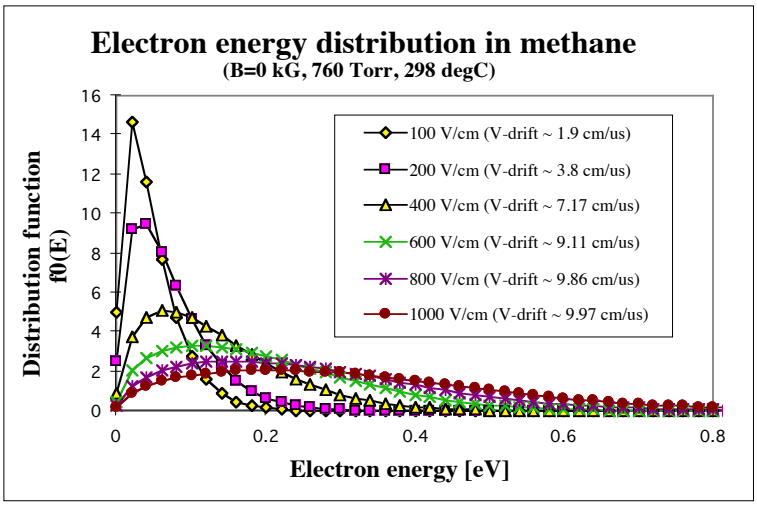

Example #2 ($f_0(\varepsilon)$ function in various gases) :

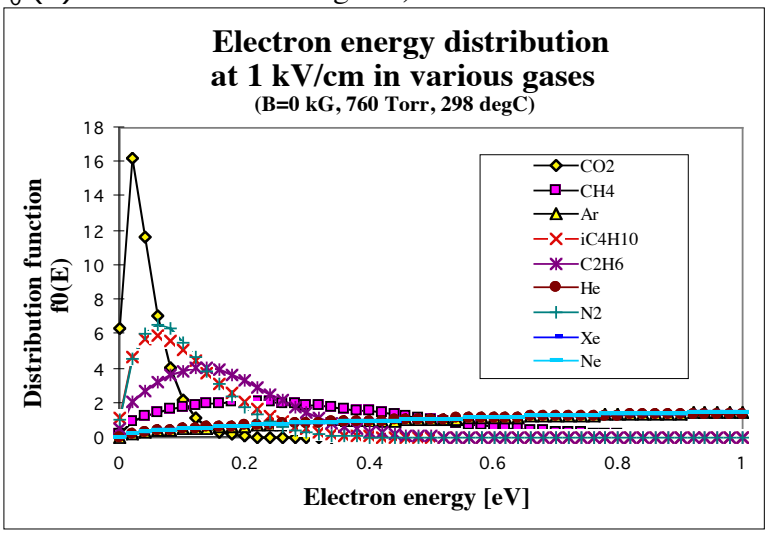

Example #3 (Calculated Lorentz angles):

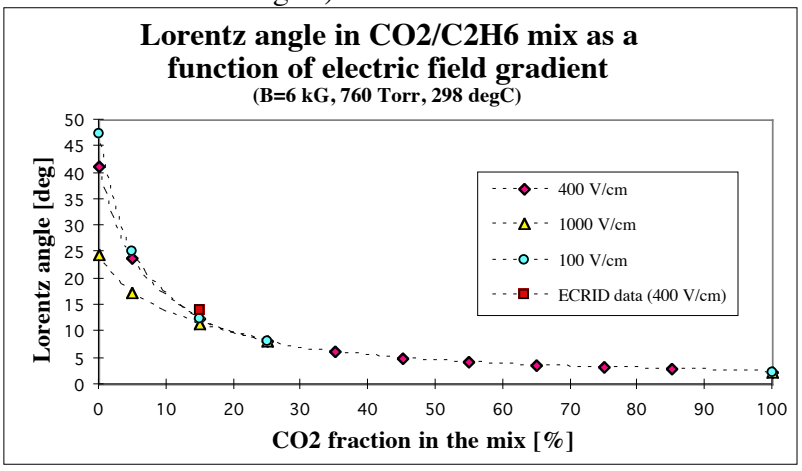

We can now predict the Lorentz angle, and therefore $\omega\tau$. However, the presented theory is not sufficiently precise in some cases because of the following arguments: (a) the presented version of the theory in this lecture does not calculate the longitudinal diffusion coefficient D_L, and (b) if we want 1% precision, the two-term approximation is not sufficient in gases with strong inelastic processes (hydrocarbons, CF_4, etc.). B. Schmidt [18] points out that to explain the data in methane it is necessary to introduce (a) six terms, (b) an anisotropy in the elastic scattering and (c) introduce higher order of vibration cross-sections - see his results on Figs 3 and 4. However, Schmidt's theory does not include the ionization and attachment processes. This particular problem was done, for example, by S. Biagi [23].

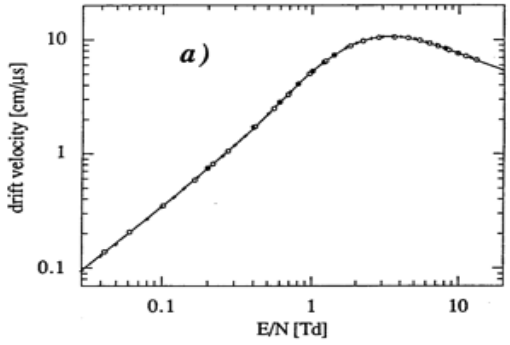

Fig.3 - Drift velocity in methane.

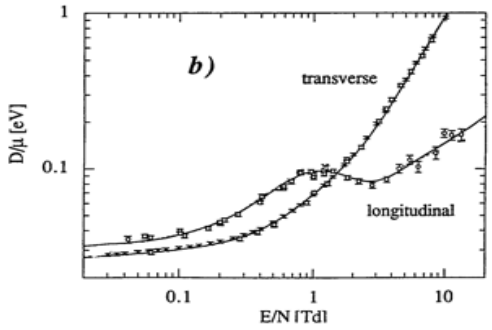

Fig.4 - Diffusion coefficient in methane.

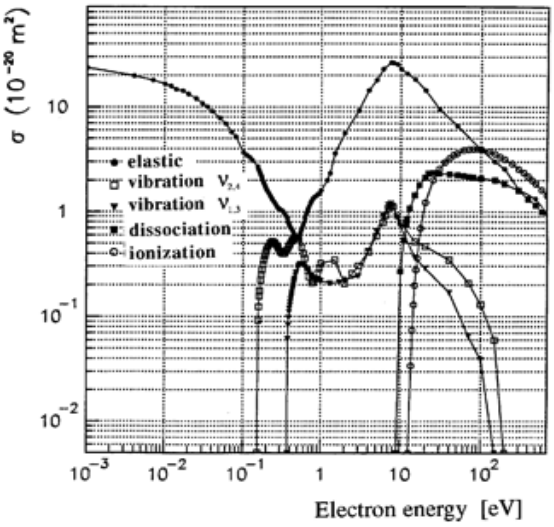

Fig.5 - Electron molecule cross-sections in methane.

3.5. Monte Carlo method.

I will mention a recent attempt by H. Pruchova and B. Franek [24]. A computer program follows the electrons and ions in small steps (fraction of a psec) and evaluates electrostatic forces, position and velocities of each electron and ion, and probability of various physics processes using the electron-molecule scattering cross-sections: (a) elastic scattering

(electron does not lose energy), (b) inelastic scattering (electron loses energy), (c) ionization scattering (a new electron is produced), (d) attachment scattering (electron is absorbed by a molecule), etc. - see Figs. 5-9 (one should also mention that similar attempts were made earlier, for example, by J. Groh [25], and by M. Matobe et al.[26]).

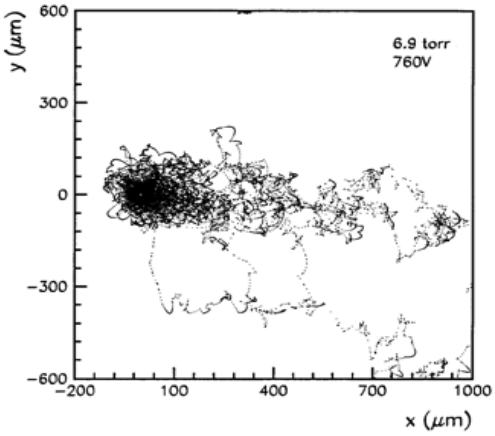

Fig.6 - Electron paths in xy-plane.

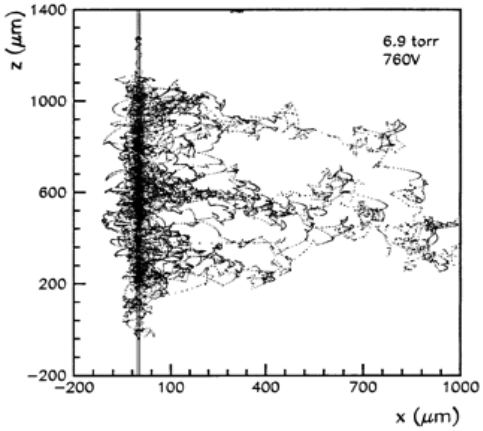

Fig.7 - Electron paths in xz-plane.

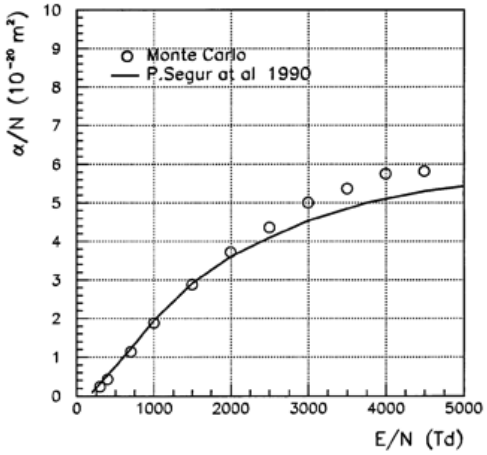

Fig.8 - Prediction of the 1-st Townsend ionization coefficient using the Monte Carlo and the Boltzmann equation methods.

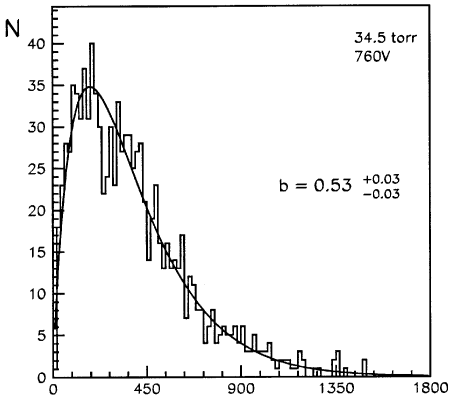

Fig.9 - Gas gain.

Difficulties of the Monte Carlo method:

1. Very demanding on the CPU time.
2. It is difficult to obtain the "correct" cross-sections. Methane is about the best studied gas of all. Some cross-sections in literature are altered to obtain the best match between theory and data using the Boltzmann equation procedure. There is some risk that the incorrectly "tuned" cross-sections would yield inconsistencies if used in the Monte Carlo method.

3. Still some difficulties to predict the practical quantities such as drift velocity, diffusion, etc., even in methane. Nevertheless, the results are still impressive.

More work is needed in this area !

Chapter 4:

4.1. Gain - phenomenological parametrization

The multiplication of ionization is described by the 1-st Townsend ionization coefficient α, which is defined as the mean number of secondary electrons produced by a free electron per centimeter of its path. The increase of the number of electrons dN per path dr is given by:

$$dN = N\ \alpha\ dr \tag{4.1}$$

No simple general expression for α exists; it has to be measured for every gas mixture. It can be shown experimentally that α is proportional to gas density ρ, provided that we keep E/ρ fixed:

$$\alpha = f(E/\rho)\ \rho \tag{4.2}$$

The amplification gain on the wire is given by the integration of equation (4.1) between the point r_c where the field is sufficient to start the avalanche and the anode radius r_a :

$$G = \frac{N}{N_0} = \exp \int_{r_c}^{r_a} \alpha(r)\ dr = \exp \int_{E(r_c)}^{E(r_a)} \alpha(E) \frac{\partial r}{\partial E} dE \tag{4.3}$$

where N & N_o is final and initial number of electrons in the avalanche, $\partial E/\partial r$ is the electric field gradient, $E(r_a)$ is the electric field on the surface of the anode wire and $E(r_c)$ is the electric field at critical radius beyond which the field is too low to support charge multiplication.Electric field near an anode wire whose radius is small compared to the inter-electrode distances is determined from equation (1.9). Inserting equation (1.5) into (4.3):

$$G = \frac{N}{N_0} = \exp \int_{E(r_c)}^{E(r_a)} \alpha(E) \frac{\lambda}{2\pi\varepsilon_0 E^2} dE \tag{4.4}$$

In a homogeneous electric field, such in the parallel plate chamber with a gap L, the equation (4.2) gives a simple expression $G = N/N_0 = \exp(\alpha L)$.

4.2. Parametrization of α

4.2.1. The Diethorn parametrization [27]:

He approximates α as follows:

$$\alpha(E) = \beta E \tag{4.5}$$

This approximation is valid for noble gases for electric field between 10^2-10^3 [V/cm Torr], a typical range of fields near the thin anode wires. Inserting equation (4.5) into (4.4):

$$\ell n\ G = \int_{E(r_c)}^{E(r_a)} \alpha(E)\,\frac{\lambda}{2\pi\varepsilon_0 E^2}\,dE = \frac{\lambda}{2\pi\varepsilon_0}\int_{E(r_c)}^{E(r_a)} \frac{\beta}{E}\,dE = \frac{\beta\lambda}{2\pi\varepsilon_0}\,\ell n\,\frac{\lambda}{2\pi\varepsilon_0 r_a E(r_c)} \qquad (4.6)$$

Potential difference between $r = r_a$ and $r = r_c$:

$$\phi(r_a) - \phi(r_c) = \int_{r_a}^{r_c} E(r)\,dr = \frac{\lambda}{2\pi\varepsilon_0}\,\ell n\,\frac{r_c}{r_a} = \frac{\lambda}{2\pi\varepsilon_0}\,\ell n\,\frac{\lambda}{2\pi\varepsilon_0 r_a E(r_c)} \qquad (4.7)$$

Assuming that it takes energy $e\,\Delta V$ in average to produce one more electron, the potential difference $\phi(r_a) - \phi(r_c)$ gives rise to Z generations:

$$G = 2^Z, \qquad Z = \frac{\phi(r_a) - \phi(r_c)}{\Delta V} \qquad (4.8)$$

This results in:

$$\ell n\ G = \frac{\ell n\,2}{\Delta V}\,\frac{\lambda}{2\pi\varepsilon_0}\,\ell n\,\frac{\lambda}{2\pi\varepsilon_0 r_a E(r_c)} \qquad (4.9)$$

Therefore $\beta = \ell n\,2/\Delta V$. Using equations (4.2), (4.4) and (4.9) we get **the final Diethorn formula:**

$$\ell n\ G = \frac{\ell n\,2}{\Delta V}\,\frac{V}{\ell n(r_a / r_a)}\,\ell n\,\frac{V}{\ell n(r_c / r_a)\, r_a\, E(r_c, \rho_0)(\rho/\rho_0)} \qquad (4.10)$$

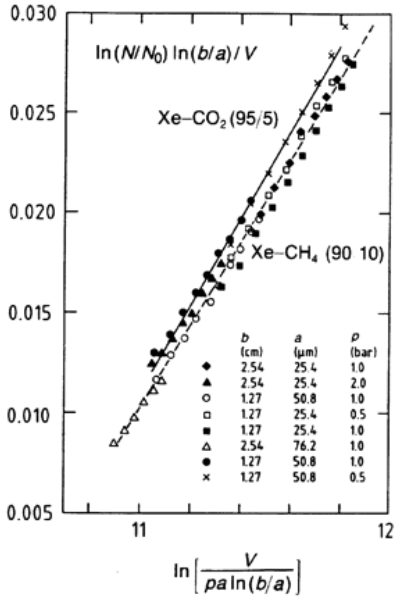

Fig.1 - Diethorn plot ($p = \rho / \rho_0$); different wire diameters fall on the same curve for a given gas - this allows scaling from one design to another.

1) Experimentally we vary $p = \rho/\rho_0$, a and $V/\ell n(r_c / r_a)$, and measure G**.**

2) A plot of $\frac{1}{V}\ell n\, G\ \ell n(r_c / r_a)$ versus $\ell n\,[V/\ell n(r_c / r_a) r_a\,(\rho/\rho_0)]$ must be linear and yields two constants ΔV and $E(r_c,\rho_0)$ - see Fig.1.

Table#1 - Examples of measured Diethorn parameters for several gases:

Gas mixture	$E(r_c)$ [kV/cm]	ΔV [Volts]
90% Ar + 10% CH_4	48 ± 3	23.6 ± 5.4
95% Ar + 5% CH_4	45 ± 4	21.8 ± 4.4
92.1% Ar + 7.9% CH_4	47.5	30.2
23.5% Ar + 76.5% CH_4	196	36.2
9.7% Ar + 90.3% CH_4	21.8	28.3

Note: ΔV and $E(r_c)$ can be considered fundamental gas constants

Application of the Diethorn formula:

a) **Dependence of gain on gas density:**

This is especially important for chambers operating at atmospheric pressure (the gas density is proportional to it). From equation (4.10) we obtain:

$$\frac{dG}{G} = -\frac{\lambda\,\ell n2}{\Delta V\,2\,\pi\,\varepsilon_0}\frac{d\rho}{\rho} \qquad (4.11)$$

The factor that multiplies $d\rho/\rho$ ranges typically between 5 and 8.

b) **Dependence of gain on geometry, voltage and space charge:**

All these effects change the local charge density of the wire λ. This in turn changes the wire gas gain as follows:

$$\frac{dG}{G} = (\ell n\, G + \frac{\lambda\,\ell n2}{\Delta V\,2\,\pi\,\varepsilon_0})\frac{d\lambda}{\lambda} \qquad (4.12)$$

The factor that multiplies $d\lambda/\lambda$ ranges typically between 10 and 20.

4.2.2. The Zastawny parametrization [28]**:**

This parametrization is valid over larger range of S, i.e. it is more general compared to Diethorn's parametrization. First, **introduce a new variable** $S(r) \equiv E(r)/\rho$**,** where E is electric field intensity and ρ is gas density. Values S_a and S_c correspond to $r = r_a$ (anode surface) and $r = r_c$ (beginning of amplification, i.e. $\alpha(r) = 0$ for $r > r_c$). In the cylindrical geometry:

$$S(r) \equiv \frac{E(r)}{\rho} = \frac{1}{\rho}\frac{E_a\, r_a}{r} = \frac{S_a\, r_a}{r} \qquad (4.13)$$

Equation (4.3) can then be rewritten:

$$\ell n\, G = \int_{r_c}^{r_a}\alpha(r)\,dr = \int_{S_c}^{S_a}\alpha\frac{\partial r}{\partial S}\,dS = \rho\, r_a\, S_a\int_{S_c}^{S_a}\frac{\alpha}{\rho}\frac{1}{S^2}\,dS \qquad (4.14)$$

Based on equation (4.2), α/ρ is a function of S only. We introduce so called **"reduced gas gain" Ψ:**

$$\Psi \equiv \frac{\ell n\, G}{\rho\, E_a\, r_a} = \int_{S_c}^{S_a} \frac{\alpha}{\rho}\frac{1}{S^2}\, dS = f(S_a) \qquad (4.15)$$

The reduced gas gain Ψ is only a function of variable S_a - see Fig. 2.

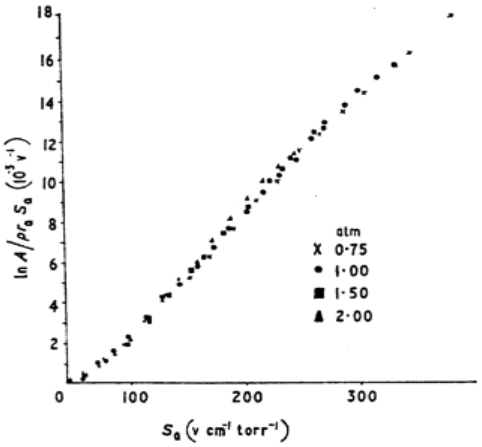

Fig.2 - Reduced gas gain $\Psi = f(S_a)$ in CO_2 gas.

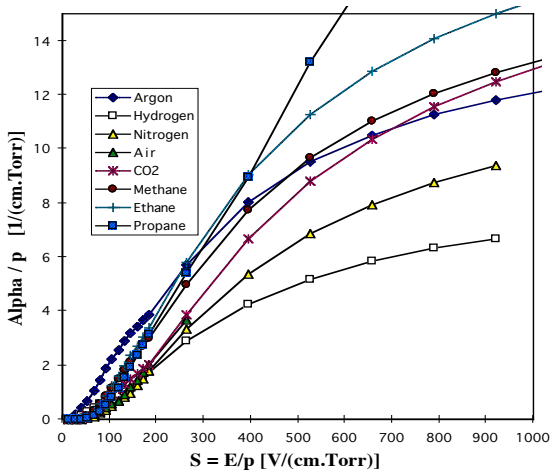

Fig.3 - The first Townsend coefficient $\alpha/\rho = f(S)$.

This is a significant result ! All data are following one single curve for a given gas choice, independent of gas pressure, voltage or anode radius. This is used to predict the gas gain in a new drift chamber geometry: (a) we parametrize the "reduced gas gain" $\psi = f(S_a)$ in a known geometry such as a tube wire chamber, (b) then we scale it to any other geometry, provided that we can calculate S_a in this geometry. This allows to know the gas gain when we simulate the drift chamber geometry in the electrostatic program.

Zastawny parametrized α as follows (in fact this is an old Korff parametrization [29]):

$$\frac{\alpha}{\rho} = A \exp\left(-\frac{B}{S}\right) \qquad (4.16)$$

where for a given gas choice, A and B are constants only in certain E/p intervals (typically 2-3 intervals). In this parametrization the **"reduced gas gain"** ψ has the following simple form:

$$\Psi \equiv \frac{\ell n\, G}{\rho\, E_a\, r_a} = \int_{S_c}^{S_a} \frac{\alpha}{\rho}\frac{1}{S^2}\, dS = f(S_a) = A \exp\left(-\frac{B}{S_a}\right) \qquad (4.17)$$

Fig. 3 shows an example of author's calculations of α using Zastawny's fits to his data.

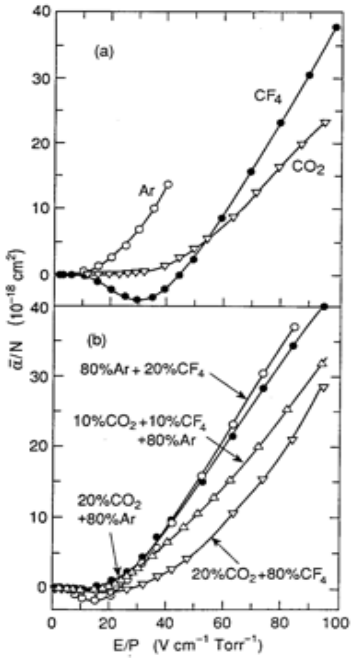

Fig.5 - The effective ionization coefficient $\bar{\alpha}/p$ or CF_4 gas is [30].

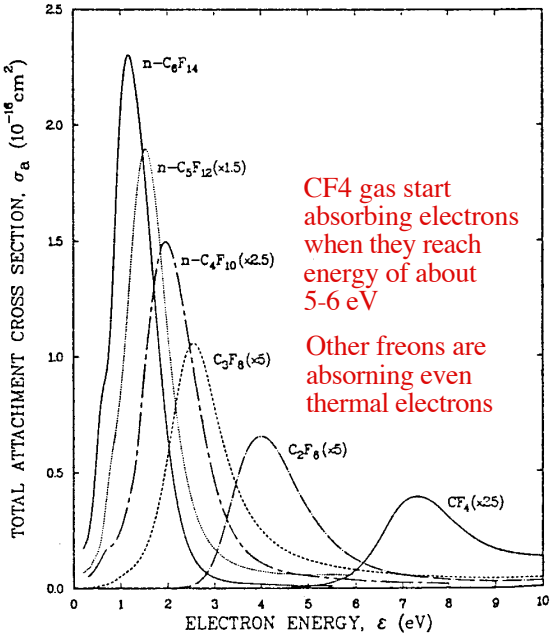

Fig.6 - The attachment cross-sections in Freons.

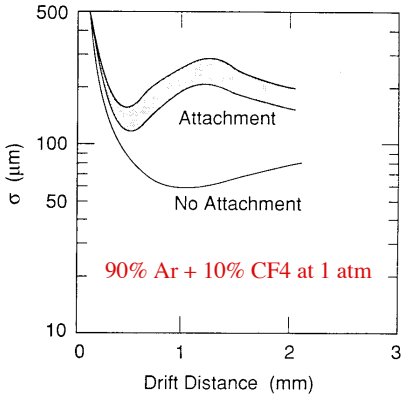

Fig.7 - Monte Carlo simulation of the resolution in 4 mm straw tube.

4.3. Gain in the presence of electron attachment

In this case one introduces **the attachment coefficient** η**,** and the gain equation (4.2) is modified as follows:

$$G = \frac{N}{N_0} = \exp \int_{r_c}^{a} (\alpha(r) - \eta(r))\, dr \qquad (4.18)$$

where $\bar{\alpha} \equiv \alpha(r) - \eta(r)$ **is the effective ionization coefficient.** From Fig. 5 one can see that we need to add some gas to CF_4, for example iC_4H_{10}, to eliminate its absorption of electrons for: 10 kV/cm < E/p < 35 kV/cm. The explanation of this effect can be traced to the attachment

cross-section in fluorocarbons - see Fig. 6. Is this significant for the practical applications ? Yes, it can affect the "near wire resolution" in detectors such as tube wire chambers [31] - see Fig. 7.

4.4. Statistical fluctuation of the gas gain

The total charge developed during a pulse is proportional to:

$$Q = n_0 \, e \, M \tag{4.19}$$

where n_o=E/W is the number of individual avalanches, E is the energy deposited by the incident radiation, W is the energy required to form one ion pair, M is the average multiplication factor and e is the electron charge. The average multiplication factor from all the avalanches which contribute to a given pulse is:

$$M = \frac{1}{n_0} \sum_{i=1}^{n_0} A_i \equiv \overline{A} \tag{4.20}$$

where eA_i is the charge contributed to the i-th avalanche. The pulse amplitude, which is proportional to Q, is subject to fluctuations because of fluctuations in n_0 and M :

$$(\frac{\sigma_Q}{Q})^2 = (\frac{\sigma_{n_0}}{n_0})^2 + (\frac{\sigma_M}{M})^2 \tag{4.21}$$

where σ_M can be rewritten as:

$$\sigma_M{}^2 = (\frac{1}{n_0})^2 \sum_{i=1}^{n_0} \sigma_{\overline{A}}^2 = \frac{1}{n_0} \, \sigma_{\overline{A}}^2 \tag{4.22}$$

Combining equations (4.21) and (4.22):

$$(\frac{\sigma_Q}{Q})^2 = (\frac{\sigma_{n_0}}{n_0})^2 + \frac{1}{n_0} (\frac{\sigma_{\overline{A}}}{\overline{A}})^2 \tag{4.23}$$

1. **Variation in the number of ion pairs:**

$$(\frac{\sigma_{n_0}}{n_0})^2 = \frac{F}{n_0} \tag{4.24}$$

where F is so called **Fano factor** (typically 0.05-0.20).

2. **Variation in single electron avalanches:**

The distribution follows the **Polya distribution** (proposed by Byrne [32])**:**

$$P(A) = [\frac{A(1+\theta)}{\overline{A}}]^{\theta} \exp[-\frac{A(1+\theta)}{\overline{A}}] \tag{4.25}$$

which has a variance $(\sigma_{\overline{A}} / \overline{A})^2 = 1/\overline{A} + b$, $b \equiv (1+\theta)^{-1}$, b is typically 0.5 and the parameter θ has a value between 0 and 1 - see Fig.3. At small E/p the parameter θ approaches zero, i.e. the distribution is **t**he exponential (so called **Furry distribution**, which has a variance $(\sigma_{\overline{A}} / \overline{A})^2 = 1$)**:**

$$P(A) = \frac{1}{\overline{A}} \exp(-\frac{A}{\overline{A}}) \tag{4.26}$$

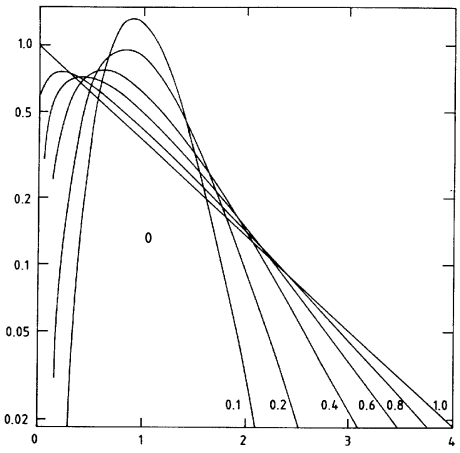

Fig.3 - Polya distributions as a function of $A / \bar{A}$ for various values of the parameter $b \equiv (1+\theta)^{-1}$; ($b = 1$ corresponds to $\theta = 0$).

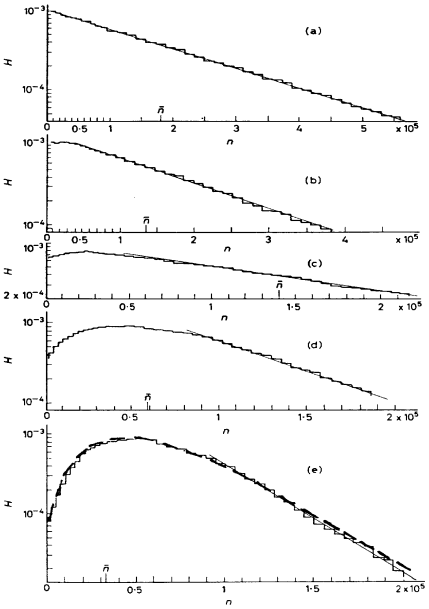

Fig.4 - Single electron pulse height spectra measured by Schlumbohm for various values of χ: (a) χ=26, (b) χ=22.6, (c) χ=10.5, (d) χ=5.3 and (e) χ=4.1.

Raether [33] suggested that the critical quantity to decide the shape of the Polya distribution is:

$$\chi = \frac{eE/\alpha}{eV_{ion}} \qquad (4.27)$$

where α is the 1-st Townsend coefficient, $1/\alpha$ is the mean free path, eE/α is the energy gained between two subsequent collisions and eV_{ion} is the ionization energy. For $\chi > 25$ the pulse height spectrum tends to exponential ($\theta \sim 0$), for $\chi < 20$ the pulse height spectrum exhibits a turnover ($\theta > 0$). Fig.3 shows the pulse height measurement in avalanches started by single electrons as measured by Schlumbohm [34], in methylal, in parallel-plate geometry - see Fig.4.

From the last chapter about the detector problems we will see that this is not the whole story. The parameter θ can be negative if the detector has problem with quenching, i.e. if the an avalanche has a tendency to breed the secondary avalanches.

The amplification on the wire **is non-linear** at large gains - see Fig. 5. At a gain of about 1.5×10^8 the limited streamer regime starts where the output pulse height does not depend any more whether the initial charge is only one electron or 220 electrons. One can also see the non-linearity of the output earlier.

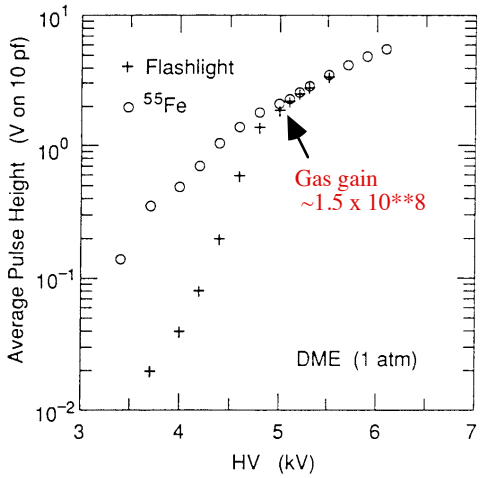

Fig.5 - Gain in a wire tube chamber as a function cathode voltage for a) Fe^{55} source (~220 el. deposited), and b) single electron source [36].

The non-linearity of charge amplification on the wire is good because it limits the gas gain and prevents the development of a spark (see last chapter). This is not so in the parallel plate chamber which tends to be more linear in this respect.

Examples of gas gain for typical anode surface gradients (E_a):

1. The gas gain as a function of the electric field on the anode surface (**Fe^{55} source**):

Gas	**Gas pressure**	**Total wire gain**	**E_a** [kV/cm]	**Wire dia.** [μm]
90% Ar+10% CH_4	1 atm	~10^4	~200	20
90% Ar+10% CH_4	1 atm	~10^5	~240	20
90% Ar+10% CH_4	4 atm	~$4x10^4$	~320	25
90% Ar+8% CH_4+2% C_4H_{10}	4 atm	~$4x10^4$	~360	20
90% Ar+8% CH_4+2% C_4H_{10}	4 atm	~$4x10^4$	~309	25
90% Ar+10% C_4H_{10}	6.1 atm	~10^5	~760	7.8
50% Ar+50% C_2H_6	1 atm	~$5x10^4$	~275	20

2. The gas gain at 1 atm as a function of the electric field on the anode surface of a 20μm anode wire (**single electron source**) [35]:

Gas	Parameter θ	Visible wire gain	E_a [kV/cm]
50% Ar+50% C_2H_6	0.252 ± 0.026	~5x10^5	~311
95% CF_4+5% DME	0.272 ± 0.044	~9.2x10^5	~377
80% CF_4+20% C_4H_{10}	0.624 ± 0.043	~3.4x10^5	~349
90% CF_4+10% CH_4	0.222 ± 0.042	~6.3x10^5	~396
50% He+50% C_2H_6	0.287 ± 0.019	~2.9x10^5	~302
78% He+15% CO_2+7% C_4H_{10}	-0.031 ± 0.019	~5.8x10^5	~283
50% Ar+50% C_2H_6	0.252 ± 0.026	~5x10^5	~311
96.4%He+3.6%DME	-0.897 ± 0.050	1.9x10^4	~188
80.5%He+19.5%DME	0.321 ± 0.058	4.1x10^5	~264
100% DME	1.768 ± 0.079	2.6x10^4	~188

Chapter 5:

5.1. Creation of the electrical signal

Moving charges create electrical signals on nearby electrodes [2]**.** Avalanche electrons have to travel only few tens of microns, positive ions travel much larger distance toward the cathode. Energy ε of the electrostatic field of the capacitor is:

$$\varepsilon = 1/2\, Q_0\, V\,, \qquad (5.1)$$

where V is potential of the capacitor and Q_o is its charge. A small charge q that travels between two points 1 and 2 under the influence of the field E changes the electric energy ε of the capacitor by the amount:

$$\Delta\varepsilon = \int_1^2 q\,\vec{E}.d\vec{r} = q(V_1 - V_2) = q\,\Delta V\,, \qquad (5.2)$$

This change in energy $\Delta\varepsilon$ of the capacitor is the source of the anode signal. The signal shape depends on the nature of the electrical configuration - see Fig. 1.

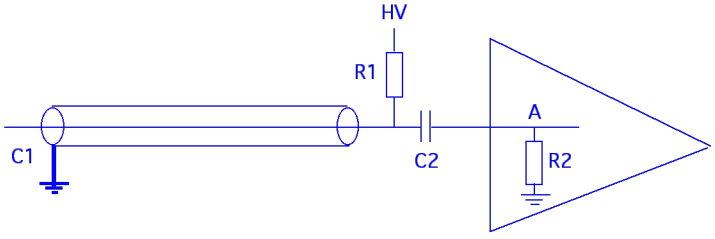

Fig.1 - A simple equivalent circuit of a tube wire detector.

There are two limiting cases:

a) The potential of the wire is re-established during the development of the pulse, which requires that charges flow quickly enough into the detector, which acts as a current source. In this case it is required that time constant R2.C1 is small compared to the pulse rise-time. The signal is the current I(t) that flows through R2. Using equation (5.1), the change in energy $\Delta\varepsilon = (1/2)\Delta Q_0(t)\,V$ of C1 capacitor causes a current flow through R2 resistor:

$$I(t) = d/dt[\Delta Q_0(t)] = (2/V)\,d/dt[\Delta\varepsilon] \qquad (5.3)$$

b) The potential of the wire is not re-established quickly because charges are not flowing quickly enough into the detector. This results in a drop of wire potential of the detector, which acts as a voltage source. In this case time constant R2.C1 is large compared with the pulse rise-time. We have a voltage pulse on R2 resistor :

$$\Delta V = 2/Q_0\,\Delta\varepsilon \qquad (5.4)$$

In practice, we are typically closer to the case (a). I give two examples:

1) CRID detector:

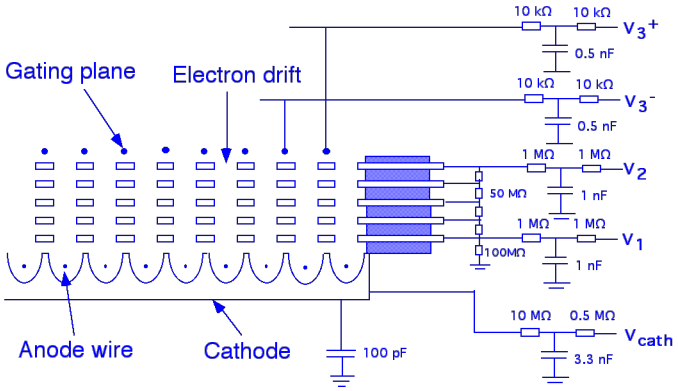

2) OPAL drift chamber:

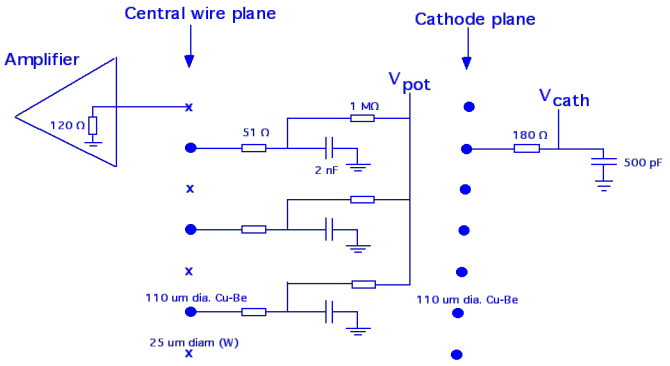

Let's consider an example of the cylindrical wire tube. I will show that the contribution of the charge motion of the electrons can be neglected [1]**.** To obtain a signal from the motion of a charge q over a distance dr, we consider a case (b) discussed above, and equations (5.4) and (1.9):

$$dV = \frac{2}{Q_0} d\varepsilon = 2\frac{q\,E(r)\,dr}{Q_0} = \frac{2q}{2\pi\varepsilon_0 L}\,\frac{1}{r}\,dr \qquad (5.5)$$

Assuming that all ion pairs are created at a distance d from anode, we obtain a contribution from electron and ion motions separately by integrating equation (5.5):

electrons:
$$\Delta V^- = \frac{2q}{2\pi\varepsilon_0 L}\int_{r_a}^{r_a+d}\frac{1}{r}dr = \frac{2q}{2\pi\varepsilon_0 L}\ell n\frac{r_a+d}{r_a} \qquad (5.6)$$

ions:
$$\Delta V^+ = \frac{2q}{2\pi\varepsilon_0 L}\int_{r_a+d}^{r_c}\frac{1}{r}dr = \frac{2q}{2\pi\varepsilon_0 L}\ell n\frac{r_c}{r_a+d} \qquad (5.7)$$

Total induced signal on anode is then:
$$\Delta V = \Delta V^- + \Delta V^+ = \frac{2q}{2\pi\varepsilon_0 L}\ell n\frac{r_c}{r_a} = \frac{2q}{C} \qquad (5.8)$$

where C is the total capacitance of this detector is:
$$C = \frac{Q_0}{V_0} = 2\pi\varepsilon_0 L\frac{1}{\ell n r_c/r_a} \qquad (5.9)$$

From here it follows that to get as large a signal as possible, one wants to keep the detector capacitance C1 in Fig. 1 as low as possible. Because d is only few tens of microns, the signal due to electron motion is much smaller than the signal due to positive ions. Therefore, the electron signal is neglected in our considerations. The time dependence of the motion of positive ions is estimated as follows:
$$v_{ion\,drift}(t) = \frac{dr(t)}{dt} = \mu^+\frac{E(r)}{p} = \frac{\mu^+ C V_0}{2\pi\varepsilon_0 L p}\,\frac{1}{r} \qquad (5.10)$$

where μ^+ is the ion mobility and p is the gas pressure. By integrating equation (12), and assuming that μ^+~conts., we obtain:
$$r(t) = r_a\sqrt{1+\frac{t}{t_0}}\,, \qquad (5.11)$$

where t_0 is the **characteristic time** of the chamber:
$$t_0 = \frac{\pi\varepsilon_0 L p r_a^2}{\mu^+ C V_0} = \frac{r_a}{2\mu^+ E(r_a)} \qquad (5.12)$$

The characteristic time, typically 0.1-2 ns, is expressed in terms of the wire radius, ion mobility and electric field on the surface of the wire. Using equations (5.2) and (1.5), we calculate the change in energy $\Delta\varepsilon$ as a function time from the motion of charge q representing the positive ions starting at anode radius and ending at radius r(t):

$$\Delta\varepsilon = \int_{r_a}^{r(t)} q\vec{E}.d\vec{r} = \int_{r_a}^{r(t)} q\frac{\lambda}{2\pi\varepsilon_0}\frac{1}{r}.d\vec{r} = \frac{q\lambda}{2\pi\varepsilon_0}\ell n\frac{r(t)}{r_a} = \frac{q\lambda}{4\pi\varepsilon_0}\ell n(1+\frac{t}{t_0}) \qquad (5.13)$$

For normalization purposes, it is useful to calculate the total energy change (using equations (1.8) and (5.13)):

$$\Delta\varepsilon\big|_{tot} = \int_{r_a}^{r_c} q\vec{E}.d\vec{r} = \frac{q\lambda}{2\pi\varepsilon_0}\ell n\frac{r_c}{r_a} = q\,V_0 \qquad (5.14)$$

This allows us to re-write equation (5.13) as follows:

$$\Delta\varepsilon = \frac{q\lambda}{4\pi\varepsilon_0}\ell n(1+\frac{t}{t_0}) = q\,V_0\ \ell n(1+\frac{t}{t_0})\,[1\Big/2\ \ell n\frac{r_c}{r_a}] = q\,V_0\ F(t) \qquad (5.15)$$

Going back to our earlier discussion related to Fig.1, and using equations (5.3) and (5.4):

Case (a) - **current pulse:**

$$I(t) = \frac{d}{dt}\Delta Q(t) = \frac{2}{V}\frac{d}{dt}\Delta\varepsilon = \frac{2}{V}\frac{q\lambda}{4\pi\varepsilon_0}\frac{1}{t+t_0} = [q\Big/\ell n\frac{r_c}{r_a}]\ \frac{1}{t+t_0} \qquad (5.16)$$

Case (b) - **voltage pulse:**

$$\Delta V = \frac{2}{Q_0}\Delta\varepsilon = \frac{2}{Q_0}q\,V_0\,\ell n(1+\frac{t}{t_0})\frac{1}{2\ \ell n\frac{r_c}{r_a}} = \frac{2q}{C}\ell n(1+\frac{t}{t_0})\frac{1}{2\ \ell n\frac{r_c}{r_a}} = \frac{2q}{C}F(t) \qquad (5.17)$$

5.2. Pulse shape prediction

5.2.1. - CRID photon detector with an amplifier [37] - see Figs. 3 and 4.

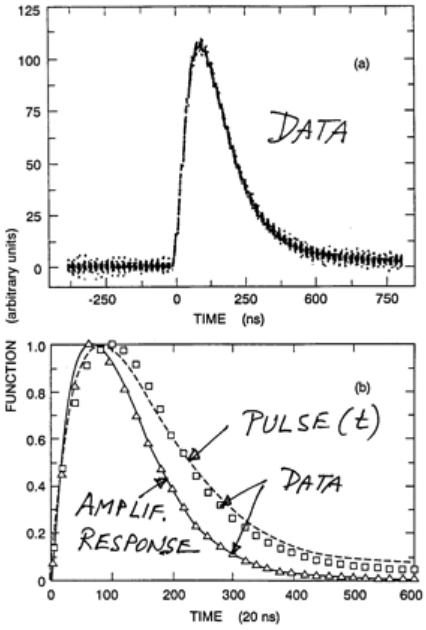

Fig. 3 - (a) Measured chamber single electron pulses, (b) measured and

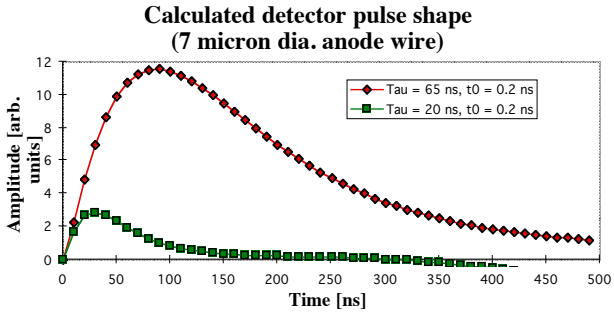

Fig. 4 - The effect of the shaping time on pulse height.

calculated amplifier response to an
impulse charge and the chamber pulse.

In this case the avalanche is initiated by a single electron created by a photo-ionization of a photo-sensitive molecule such as TMAE or TEA. The pulse is the result of a convolution of the amplifier response to the impulse charge and the positive ion response:

a) amplifier response: $t\, e^{(-t/\tau)}$, where $\tau \sim 65$ ns (shaping time),

b) positive ion response: $I(t) = (q \Big/ \ell n \frac{r_c}{r_a}) \frac{1}{t + t_0} = \frac{A}{t + t_0}$

c) Additional constants needed for the problem (for CH_4 gas): $r_c = 0.146$cm, $r_a = 3.5 \times 10^{-4}$ cm, $\mu^+(CH_4) \sim 2.26\ cm^2V^{-1}sec^{-1}$, $E(r_a) = 810$ kV/cm, $t_o = 0.1$ ns (unusually small !!; normal drift chambers have thicker wires, $t_0 \sim 1$-2 ns and $E(r_a) \sim 300$-400 kV/cm).

The convolution of two functions is the following integral:

$$Pulse(t) = A \int_0^t \frac{t',\, e^{(-t'/\tau)}}{t - t' + t_0}\, dt' = A \exp(-\frac{t + t_0}{\tau})(t + t_0). \qquad (5.18)$$

$$.\{\ell n(1 + \frac{t}{t_0}) + \sum_{n=1}^{\infty} (\frac{t_0}{\tau}) \frac{1}{n \cdot n!} [(1 + \frac{t}{t_0})^n - 1]\} - \tau [1 - \exp(-\frac{t}{\tau})]$$

The comparison between this simple theory and the measurement was done in the CRID detector operating with the CH_4 gas, the early version of the CRID amplifier was coupled to the LeCroy waveform digitizer. It is interesting to determine the influence of the shaping time on the pulse height. If CRID detector would use 20 ns shaping time, the pulse height would have been 4-5 times smaller, resulting in the necessity to increase operating cathode voltage by ~150 Volts - see Fig. 4. Running with shorter shaping time would mean a necessity to run higher voltage of about 150 V on cathode (the final CRID gas is actually C_2H_6, which gives $t_o \sim 0.2$ns for $E(r_a) = 725$ kV/cm and $\mu^+(C_2H_6) \sim 1.4\ cm^2V^{-1}sec^{-1}$).

5.2.2. - Drift chamber pulses [38]**.**

In this case the avalanche is initiated by a number of electrons arriving in clusters at slightly different times and each subject to a different avalanche fluctuation, which will create an additional randomness compared to the photon detector response. To treat this problem correctly, one has to use the Monte Carlo method. The drift chamber pulse is a result of a numerical convolution of three basic responses:

$$Pulse(t) = I_{drift}(t) \times I_{avalanche}(t) \times I_{electronics}(t), \qquad (5.19)$$

where

1. $I_{drift}(t)$ is generated by:

a) working with a correct electrostatic field,

b) creating the primary ionization,

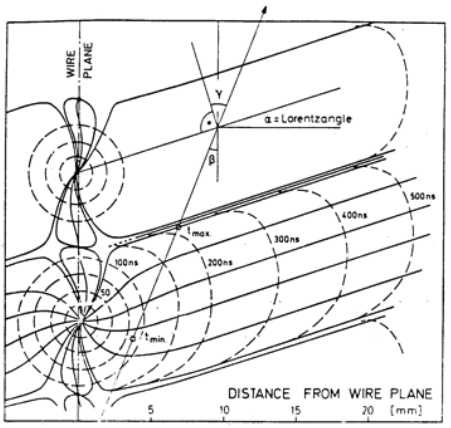

Fig. 5 - The drift in the jet chamber.

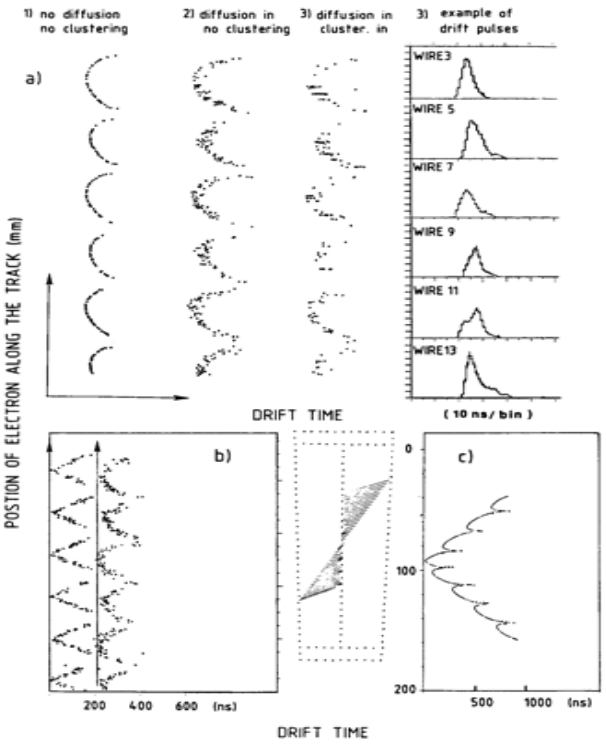

Fig. 6 - The non-isochronic charge collection in the jet chamber operating with 90%Ar+ 10%C_4H_{10} at 1 atm and 10 kG: (a) the effect of diffusion and clustering on the drift chamber pulse randomness (avalanche fluctuations and electronics included), (b) the effect of impact parameter (0 and 6 mm), (c) the effect of angle of the track (B = 0 kG).

c) drifting each electron within each cluster independently,

c) using the correct drift velocity in each step,

d) including the effect of the diffusion,

e) including the effect of the magnetic field.

2. $I_{avalanche}(t)$ is generated by:

a) including the effect of the motion of the positive ions,

b) including the effect of the avalanche fluctuations.

3. $I_{electronics}(t)$ is generated by:

a) using the measured or calculated response of the amplifier,

b) using the effect of filters, cables, noise, etc.

Why all this trouble ? My hope at that time, i.e. ~15 years ago, was to discover some new timing strategy which would allow to create a extremely high resolution drift chamber. Let's apply this simulation model to the jet chamber - see Fig. 5. The electrons do not arrive to the anode wire at the same time. This is a major factor limiting the high resolution capability for short drifts - see Fig. 6:

Question: Can we improve the non-isochronic behavior of the jet chamber by a choice of the gas operating point ?

Answer: Yes, but the magnetic field will spoil it - see Fig. 7:

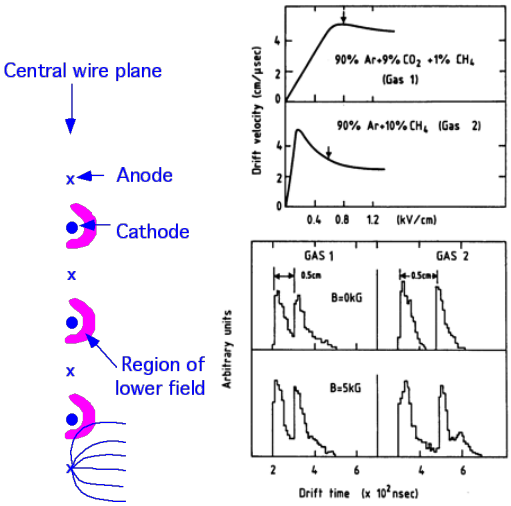

Fig. 7 - The effect of choice of operating point in the drift velocity curve on the isochrony of the jet chamber.

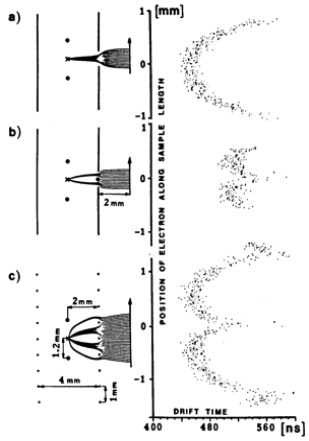

Fig. 8 - The effect of the drift geometry on the isochrony of the charge collection.

Question: Can we improve the non-isochronic behavior by a choice of geometry ?

Answer: Yes, but the magnetic field and angle of tracks will spoil it again - see Fig. 8.

5.2.3. - Propagation of signals along the wires.

First, I will show a practical example of the ~4.5 m long 8-wire prototype built during the R&D stage for the OPAL central drift chamber development [10] - see Fig. 9 and 10.

For both terminations we clearly observe reflections. The chamber impedance is of the order ~300 Ω ; a 50 Ω termination at the end is an obvious mismatch which will cause a reflection. The charge division needs a low impedance amplifier. Therefore we will have inherently the reflection in the problem, and therefore the non-linearity in the z-coordinate.

The theory in the early part of this chapter did not include one significant ingredient: the propagation of signals along the wires. Such propagation follows the **Telegrapher** equation for the system of wires:

$$\frac{\partial I_i}{\partial z} = -\sum_k C_{ik} \frac{\partial V_k}{\partial t}, \quad \frac{\partial V_i}{\partial z} = -R_i I_i - \sum_k L_{ik} \frac{\partial I_k}{\partial t} \qquad (5.23)$$

where C_{ik}, L_{ik} are wire to wire capacitance and inductance per unit length. The solution of this problem allows to design a proper drift chamber termination by minimizing the signal reflections, at least in principle. Let's discuss two possible wire terminations of the 4 m long OPAL central drift chamber [39].

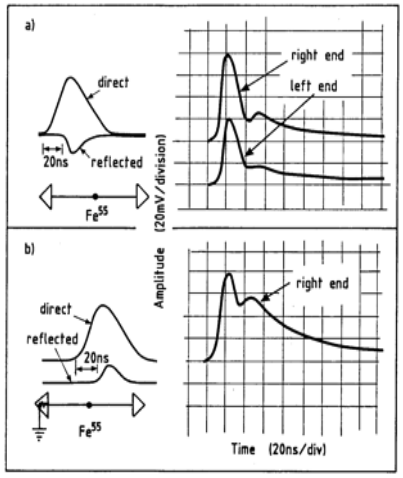

Fig. 9 - Signals of a Fe^{55} source painted on a potential wire in the middle of the chamber.(a) Low impedance at both ends (~50 Ω), (b) high impedance at left end (~MΩ).

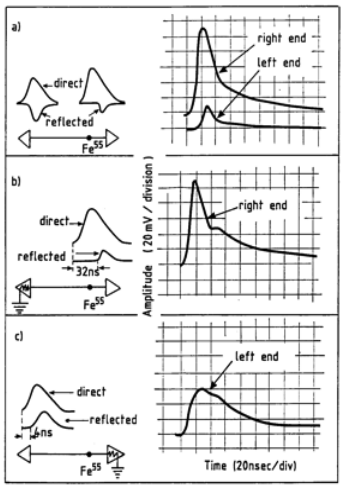

Fig. 10 - Signals of a Fe^{55} source painted on a potential wire 50 cm from the wire end. (a) Low impedance at both ends, (b) high impedance at left end, (c) high impedance at right end.

a) Simple minded termination of the OPAL full size prototype, which was "tuned" by the 8-wire prototype [10] (see Figs. 9 & 10):

TERMINATION A:

b) Termination of the final OPAL chamber after the Bock's analysis [39]:

TERMINATION B:

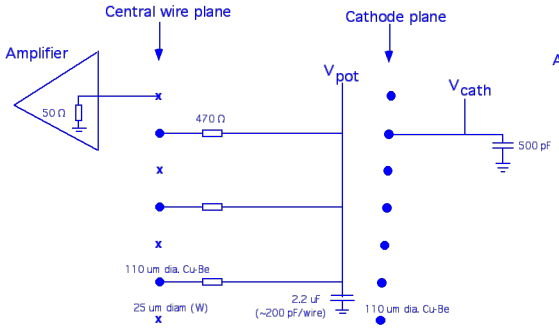

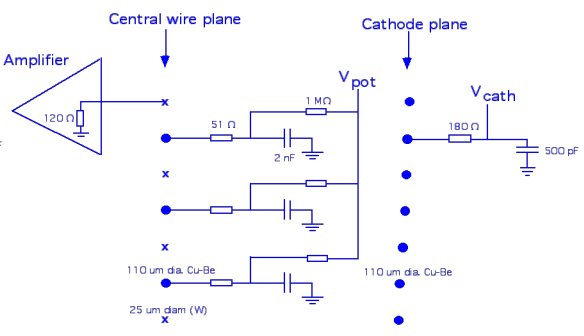

Model for the input pulse shape in the analysis (4 free parameters):

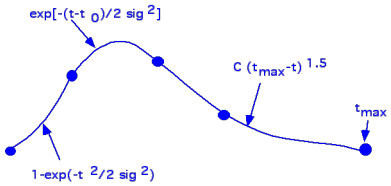

Fig. 11 shows the result of the P.Bock's calculation of the pulse shapes.

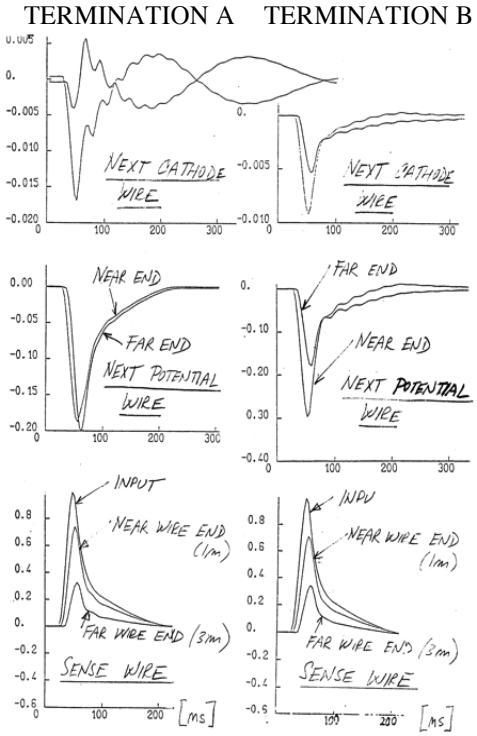

Fig. 11 - Simulated pulse shapes in a 4 m long OPAL drift chamber.

However, this termination did not remove the basic reflection problem discussed earlier, which is inherent in the problem of charge division. All it really does is to remove the 2-nd order ripple effects.

5.2.4. - currents induced on nearby electrodes.

Ramo's theorem allows us to predict the induced signal on any electrode [40]**.** It says: the instantaneous current I_i flowing into one particular electrode i due to a motion of charge q at position $\vec{r}$ with a velocity $\vec{v}(\vec{r})$ can be calculated using equation:

$$I_i = -q \frac{\vec{v}(\vec{r}) \bullet \vec{E}(\vec{r})}{V_i} \qquad (5.24)$$

where $\vec{E}(\vec{r})$ is field created by rising the electrode i to potential V_i and grounding all other electrodes, in absence of charge. A consequence of this theorem is the well known fact that the signal induced on the wire, which has an avalanche, has a sign opposite to that of the signal on the neighboring wires, which have the cross-talk.

Example:

The radioactive Fe^{55} source painted on the potential wires of the 8-wire prototype allowed also to study the wire to wire cross-talk. The cross-talk between nearest neighbors amounts to ~7%, it has the same time structure as the prompt signal and has the opposite polarity [10] - see Fig. 12**.**

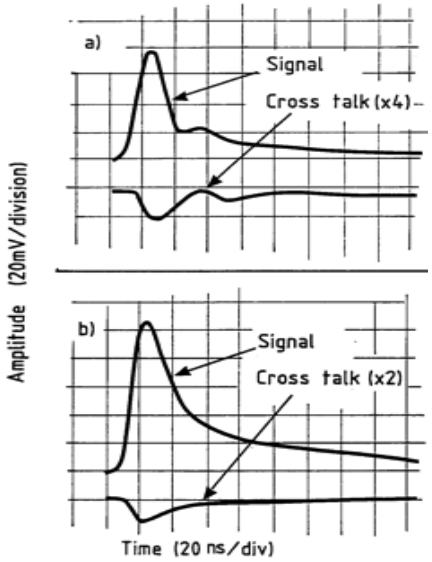

Fig. 12 - Cross-talk from one wire to the next. (a) Middle position of Fe55 source, (b) source positioned 50 cm from one wire end.

Coefficients of induction C_{ik} can be used to estimate the cross-talk from a signal on neighboring wires as follows [41].

5.2.5. - charge division.

The propagation of signals along the wire is governed by the equation:

$$\frac{\partial^2 V(z,t)}{\partial z^2} = \frac{L_w C_w}{\ell^2} \frac{\partial^2 V(z,t)}{\partial t^2} + \frac{R_w C_w}{\ell^2} \frac{\partial V(z,t)}{\partial t} \qquad (5.24)$$

where V(z,t) is voltage, Z is position along the wire (z = 0 at center), t is time, ℓ is length of the wire, R_w, L_w, C_w is wire resistance, inductance and capacitance, $L_w C_w/\ell$. The $\partial^2 V(z,t)/\partial t^2$ term represents wave propagation, $R_w C_w/\ell^2 \; \partial V(z,t)/\partial t$ represents diffusive propagation. Assuming the boundary condition $V(-\ell/2,t) = V(+\ell/2,t) = 0$, the equation (5.24) can be solved by the Fourier series method. The general solution has a form:

$$V(z,t) = \sum_{n=1}^{\infty} A_n T_n(t) \sin[\frac{n\pi z}{\ell}] \qquad (5.25)$$

Time equation then becomes

$$\frac{L_w C_w}{\ell^2}\frac{\partial^2 T_n(t)}{\partial t^2} + \frac{R_w C_w}{\ell^2}\frac{\partial T_n(t)}{\partial t} + (\frac{n\pi}{\ell})^2 T_n(t) = 0 \qquad (5.26)$$

To get some insight into the integration time needed to obtain the linear charge division, we simplify this problem by assuming [42]: (a) neglect the wave propagation by assuming that the $L_w C_w$ is small, i.e. the equation (23) becomes the diffusion equation; (b) assume that the boundary condition assumes the grounded ends, i.e. $V(-\ell/2,t) = V(+\ell/2,t) = 0$ ($z = 0$ at center); (c) we inject a δ-function charge Q at position x along the wire; (d) we detect the charge using the integrating charge amplifier.

The current flowing into charge integrated amplifier is:

$$I(z,t) = \frac{Q}{R_w C_w}\{\sum_{n=1}^{\infty} 2n\pi \exp[-\frac{t n^2 \pi^2}{R_w C_w}] \sin[\frac{n\pi z}{\ell}]\} \qquad (5.25)$$

The integrated charge $q_1(z,t)$ at one wire end after time t is:

$$q_1(z,t) = \int I(z,t)\,dt = = Q\{\frac{1}{2} + \frac{z}{\ell} + \frac{2}{\pi}\sum_{n=1}^{\infty}\frac{(-1)^n}{n} \exp[-\frac{t n^2 \pi^2}{R_w C_w}] \sin[n\pi(\frac{1}{2}+\frac{z}{\ell})]\} \qquad (5.25)$$

Clearly, the solution has transients represented by the sum. The longest lasting transient term (n = 1) decays with a time constant $R_w C_w / \pi^2$. For linear relation between $q_1(z,t)$ and the position along the wire, the sum in equation (25) should be negligible. The time required for the position non-linearity to be less than 0.2 % is $t \geq R_w C_w / 2$.

Examples of two detectors using the charge division:

a) Opal 8-wire prototype: $R_w = 850\ \Omega$, C_w = 40-50 pF, => $R_w C_w \sim 35$ns

b) CRID detector: $R_w = 40\ k\Omega$, C_w = 2-3 pF, => $R_w C_w \sim 100$ns

We will now discuss the position sensitivity and resolution of the charge division:

a) Without coupling capacitors between the wire and the amplifier (include the contact resistance between the wire and PC board).

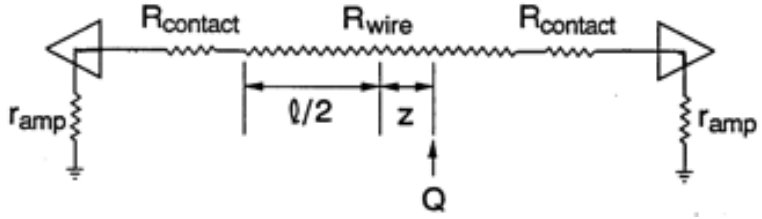

Let q_1 and q_2 be the charge reaching the preamps at each end of the wire of resistance R_w. Let $R_{contact}$ and r_{amp} are the contact resistance and amplifier input impedance. If $Q=q_1+q_2$ is the charge injected, then:

$$\frac{q_1}{q_1+q_2} = \frac{\frac{1}{2}(R_w + 2r_{amp} + 2R_{contact}) + \frac{z R_w}{\ell}}{R_w + 2r_{amp} + 2R_{contact}} = \frac{1}{2} + \frac{z}{\ell}\frac{R_w}{R_w + 2r_{amp} + 2R_{contact}} \qquad (5.26)$$

b) With coupling capacitors between the wire and the amplifier.

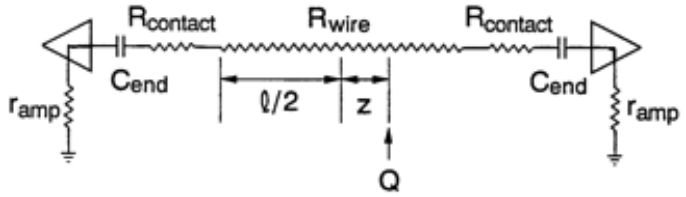

Let's assume that the charge Q divides at t = 0 such that the initial charges deposited on the capacitors are:

$$\frac{q_1(t=0)}{q_1+q_2} = \frac{1}{2} + \frac{z}{\ell}\frac{R_w}{R_w + 2\,r_{amp} + 2\,R_{contact}} \tag{5.27}$$

Usually we measure charge over a certain time period corresponding to gate T. There will be a relaxation of charge between the capacitors through the resistive wire. What is measured is a charge $q_1(T)$ and not $q_1(t=0)$. To estimate $q_1(T)$ consider the equivalent circuit below, where the charges $q_1(t=0)$ and $q_2(t=0)$ are placed on the capacitors at t = 0.

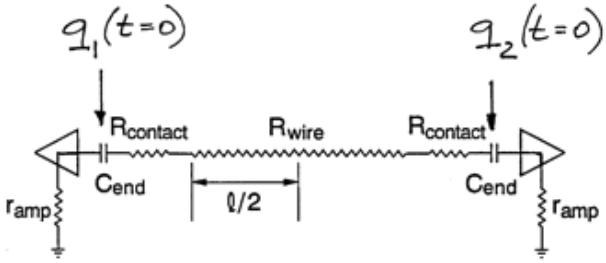

Solving the differential equation, we find:

$$\frac{q_1(T)}{q_1+q_2} = \frac{1}{2} + \frac{z}{\ell}\left(\frac{\beta\,R_w}{R_w + 2\,r_{amp} + 2\,R_{contact}}\right) \tag{5.28}$$

where

$$\beta = \exp\left[-\frac{T}{(R_w + 2\,r_{amp} + 2\,R_{contact})\,C_{end}}\right. \tag{5.29}$$

If β is small, sensitivity is lost. It is therefore mandatory that $R_w\,C_{end} >> T$. We must also require that $R_w >> r_{amp}+R_{contact}$. In typical chamber designs $\beta \sim 1$.

To get the position resolution as a function of Q and z, we use equation (5.28) and solve for z:

$$\frac{z}{\ell} = \frac{R_w + 2\,r_{amp} + 2\,R_{contact}}{2\,\beta\,R_w}\;\;\frac{q_1 - q_2}{q_1 + q_2} \tag{5.30}$$

Therefore
$$\left(\frac{\sigma_z}{\ell}\right)^2 = \left(\frac{\partial\frac{z}{\ell}}{\partial q_1}\right)^2 (\sigma_{q_1})^2 + \left(\frac{\partial\frac{z}{\ell}}{\partial q_2}\right)^2 (\sigma_{q_2})^2 + \left(\frac{\partial\frac{z}{\ell}}{\partial \beta}\right)^2 (\sigma_\beta)^2 \tag{5.31}$$

After some rearranging we obtain the following expression:

$$\left(\frac{\sigma_z}{\ell}\right)^2 = \left(\frac{\sigma_{PED}}{\sqrt{2}}\right)^2 \frac{\left[\left(\frac{R_w + 2\,r_{amp} + 2\,R_{contact}}{\beta\,R_w}\right)^2 + \left(\frac{2\,z}{\ell}\right)^2\right]}{(q_1+q_2)^2} + \left(\frac{\sigma_\beta}{\beta}\right)^2 \left(\frac{z}{\ell}\right)^2 \tag{5.32}$$

where σ_{PED} is the pedestal arising from amplifier noise, cable pick-up noise, etc. We assume that $\sigma_{PED} = \sigma_{q_1} + \sigma_{q_2}$. The resistance of the wire adds noise also, so called Johnson noise, which is a position independent noise. If we add it in quadrature, we get the final equation:

$$\left(\frac{\sigma_z}{\ell}\right) \cong \sqrt{\left(\frac{\sigma_J}{q_1+q_2}\right)^2 + \left(\frac{\sigma_{amp}/\sqrt{2}}{q_1+q_2}\right)^2 \left[\left(\frac{R_w + 2R_{contact} + 2r_{amp}}{R_w}\right)^2 + \left(\frac{2z}{\ell}\right)^2\right]} \qquad (5.33)$$

I will now discuss specifically the **CRID detector**. The Johnson noise is estimated using the following formula:

$$\sigma_J = 2.718\sqrt{\frac{kT\tau}{2(R_w + 2R_{contact} + 2r_{amp})}} \qquad (5.34)$$

where k is the Boltzmann constant; T is absolute temperature; τ is the amplifier shaping time (65 ns). The CRID amplifier noise with RC-CR shaping and with the FET input can be calculated as follows [43]:

$$\sigma_{amp} \cong 2.718\sqrt{\frac{k\ T\ R_{eq}(C_{in} + C_{ch})^2}{2\ \tau}} \qquad (5.35)$$

where R_{eq} is the equivalent noise resistance of the FET (~50 Ω), C_{in} is the amplifier input capacitance (~10 pF), C_{ch} is the detector capacitance (~15 pF), $\ell = 103.5 \pm 0.5$ mm, q_1+q_2 is the visible charge (1-2 x 10^5 el.), $R_{wire} = 41.3 \pm 2.64$kΩ, $R_{contact} = 94.6 \pm 116$Ω, $r_{amp} = 680 \pm 50$ Ω. Equations (5.34) and (5.35) yield σ_J ~ 960 and σ_{amp} ~ 530 electrons. We can now use the equation (5.33) to estimate the charge division resolution. Fig.13 compares the calculation with the data [44].

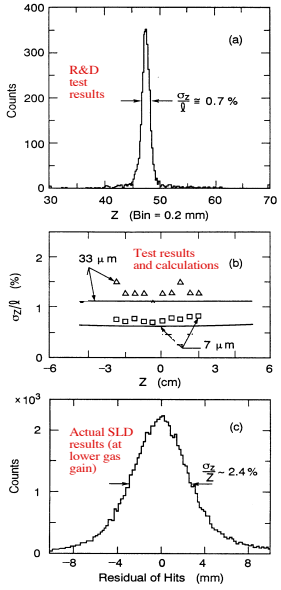

Fig. 13 - Charge division resolution.

The final z-coordinate has to take into account the gains of the amplifiers resulting in the final expression:

$$z = C \frac{g_1 q_1 - g_2 q_2}{g_1 q_1 + g_2 q_2} \frac{R_w + 2(r_{amp} + R_{contact})}{R_w} \frac{\ell}{2} \qquad (5.36)$$

where q_1, q_2 is measured charges at both ends of the wire, g_1, g_2 are calibration factors reflecting the amplifier gain variations (obtained from the special amplifier calibration runs), R_w is carbon wire resistance, r_{amp} is the amplifier impedance, $R_{conract}$ is contact resistance between the carbon wire and the PC board trace, ℓ is wire length, C is calibration factor reflecting errors in resistors, capacitors, etc. (obtained from the UV fiber calibration runs).

Chapter 6

Limit of accuracy for the high resolution drift chambers - can they compete with the silicon ?

In this chapter I will discuss a limit of highest possible resolution in the most precise drift chambers. There are two methods to estimate the high precision drift chamber resolution:

6.1. Simple estimate:

Generally, there are several major contributions to the resolution.

$$\sigma^2(x) = \sigma^2_{diffusion}(x) + \sigma^2_{ionization}(x) + \sigma^2_{track} + \sigma^2_{electronics} \qquad (6.1)$$

where $\sigma_{electronics}$ is an offset caused by the electronics noise, σ_{track} is the finite size of ionization trail left by a track, $\sigma_{ionization}(x)$ are fluctuations in primary ionization statistics, $\sigma^0_{diffusion\ near\ wire}$ is the constant term describing the diffusion near the wire in a presence of a very large field, $\sigma_{diffusion}(x)$ is the x-dependent term describing the diffusion in the middle of drift cell where the field is low. We neglect other effects, which are important for the TPC resolution, such as angle of a track in respect to wire, pad resolution, etc.; see Ref.3 for description of these effects.

(a) σ_{track} - This term is typically neglected. The primary ionization is contained within less than 2 μm of the original track direction.

Table 1 - Physical width of the track in Argon gas

%	Atomic shell	Average energy	Electron range 9.9×10^{-6} (E / keV) g cm^{-2}
~92	M-shell	≤ 30 eV	< 2 μm
~8	L-shell	≤ 400 eV	~ 20 μm
~0.1	K-shell	≤ 4 keV	~ 200 μm

(b) $\sigma_{ionization}(x)$ - This term is important near the anode wire where the number of electrons available is small and subject to ionization fluctuations.

(c) $\sigma^0_{diffusion\ near\ wire}$ - This term has not been even considered in any analysis I know so far. It has been suggested by F. Villa [45], who pointed out that the electron energy increases as a function of electric field at least quadratically, i.e. one could have significant contribution near the anode wire where the electric field is typically 200-400 kV/cm. I have decided to explore this question experimentally [35], and concluded that such term indeed could play a role in the highest resolution applications - see Fig.1. One can see that the $\sigma^0_{diffusion\ near\ wire}(1\,electron)$ term appears to be dominant. to explain the offset at $\sigma(x = 0)$. In the final application more than one electron contribute, i.e. we expect $\sigma^0_{diffusion\ near\ wire}(N\,electron) = \sigma^0_{diffusion\ near\ wire}(1\,electron)/\sqrt{N}$. For example in case of CF_4 gas, we see in Fig.1, $\sigma^0_{diffusion\ near\ wire}(1\,electron) \sim 170$ μm. In an application where we would have N~100 electrons, we expect $\sigma^0_{diffusion\ near\ wire}(N\,electron) \sim 170/\sqrt{100} = 17$ μm. This is certainly not negligible, and I should add that 100 electrons is rather unusual; typically we end up with 10-20 electrons. The measurement of $\sigma^0_{diffusion\ near\ wire}(1\,electron)$ in cool gases such as DME or CO_2 does not exist at present.

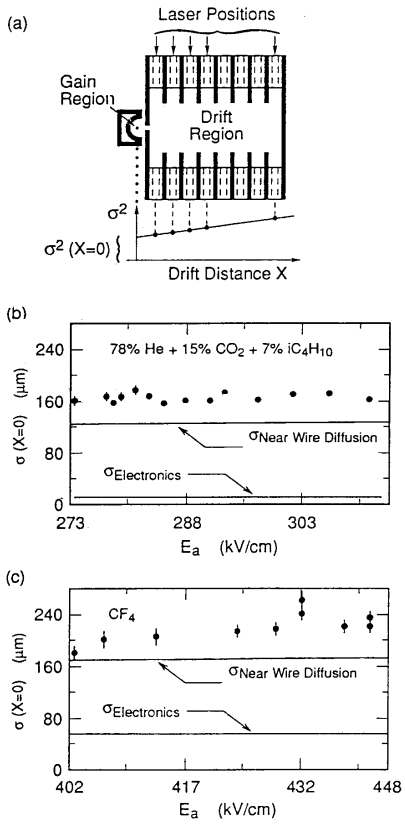

Fig. 1 - Diffusion near the wire in a presence of a very large field dominates $\sigma(x = 0)$.

(d) $\sigma_{diffusion}(x)$ - As we discussed earlier, one electron time dispersion of an original point-like charge distribution is:

$$\sigma_x(1\ \text{electron}) = \sqrt{2Dt} = \sqrt{\frac{2Dx}{\mu E}} = \sqrt{\frac{2\varepsilon_k x}{eE}} = \frac{1}{\sqrt{p}}\sqrt{\frac{2\varepsilon_k x}{e\left(\frac{E}{p}\right)}} \qquad (6.2)$$

From here we obtain four practical dependencies:

a) If $\varepsilon_k \sim$ const. and x ~ const.: $$\sigma_x(1\ \text{electron}) \sim \frac{1}{\sqrt{E}} \qquad (6.3)$$

b) If in addition E/p ~ const.: $$\sigma_x(1\ \text{electron}) \sim \frac{1}{\sqrt{p}} \qquad (6.4)$$

c) For <u>cool gases</u> ($\varepsilon_k \sim kT$): $$\sigma_x(1\ \text{electron}) = \sqrt{2Dt} = \sqrt{\frac{2kTx}{eE}} \qquad (6.5)$$

d) Because of the diffusion dependence on the drift distance x the resolution data are usually fitted by:

$$\sigma^2 = \sigma_0^2 + \delta x \qquad (6.6)$$

The resolution data are usually presented in this form to verify that other effects, such as the electron attachment, do not affect this dependence.

CO_2 and DME gases are frequently used in high precision drift chambers, because they approach the cool gas limit - see Fig. 2.

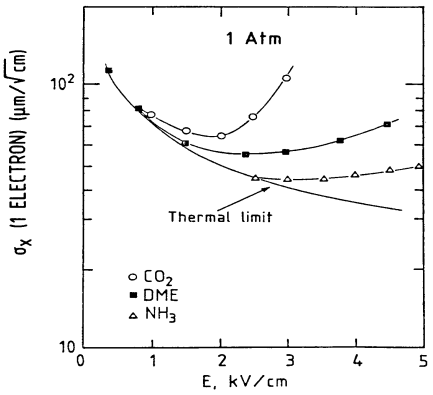

Fig. 2 - Single electron diffusion for 1 cm drift and 1 atm pressure as a function of electric field [46].

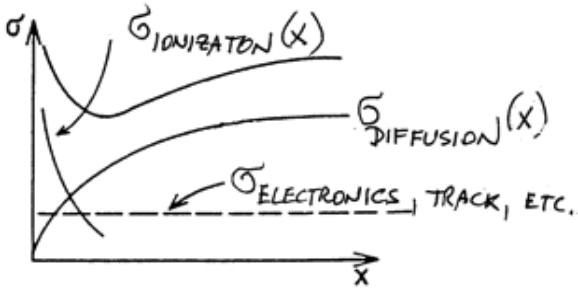

Fig. 3 - Typical contributions to the resolution as a function of drift distance.

We can see that the cool gases can reach $\sigma_x(1\ \text{electron}) \sim 50\text{-}80\,\mu\text{m}$ at 1 atm and 1 cm drift, and the transverse and longitudinal diffusions are close to each other (we assume the same). As we discussed earlier, in hot gases $\sigma_L(1\ \text{electron})$ could be as low as half of $\sigma_x(1\ \text{electron})$. Typically, in hot gases $\sigma_L(1\ \text{electron}) \sim 120\text{-}200\,\mu\text{m}$ at 1 atm and 1 cm drift. It is the longitudinal diffusion which influences the arrival time distribution.

Individual contributions in typical high precision chambers can be qualitatively described in Fig.3. The relative size of terms in equation (1) depends on the choice of gas, pressure, electronics, method of charge collection and method of analysis. For example, the $\sigma_{\text{ionization}}(x)$ term can be greatly suppressed by increasing the gas pressure.

Table 1 - Cluster size distribution in percent

k (cluster size)	CH_4	Ar	He	CO_2
1 e^-	78.6 %	65.6	76.6	72.5
2	12	15.0	12.5	14.0
3	3.4	6.4	4.6	4.2
4	1.6	3.5	2.0	2.2
5	0.95	2.25	1.2	1.4
6	0.6	1.55	0.75	1.0
7	0.44	1.05	0.50	0.75
8	0.34	0.81	0.36	0.55
9	0.27	0.61	0.25	0.46
10	0.21	0.49	0.19	0.38

11	0.17	0.39	0.14	0.34
12	0.13	0.30	0.10	0.28
13	0.10	0.25	0.08	0.24
14	0.08	0.20	0.06	0.20
15	0.06	0.16	0.048	0.16
16	0.050	0.12	0.043	0.12
17	0.042	0.095	0.038	0.09
18	0.037	0.075	0.034	0.064
> 20	$(11.9/k^2)$	$(21.6/k^2)$	$(10.9/k^2)$	$(14.9/k^2)$

Note: 20-30% of the time a cluster will have more than one electron.

6.1.1. The first electron timing:

Cramer [47] derived a formula describing time accuracy based on arrival time of the M-th electron in a given sample of N electrons. It is valid for large N, and M << N:

$$\sigma_{diffusion}(M - \text{th arriving electron}) = \frac{\sigma_L(1 \text{ electron})}{\sqrt{2\ \ell n\ N}} \sum_{i=M}^{N} \frac{1}{i^2}, \qquad (6.7)$$

which becomes for M = 1:

$$\sigma_{diffusion}(1 - \text{st arriving electron}) = \frac{\sigma_L(1 \text{ electron})}{\sqrt{2\ \ell n\ N}} \sum_{i=1}^{N} \frac{1}{i^2} \approx$$

$$\approx \frac{\sigma_L(1 \text{ electron})}{\sqrt{2\ \ell n\ N}} \sqrt{\frac{\pi^2}{6}} = \frac{0.91\ \sigma_L(1 \text{ electron})}{\sqrt{\ell n\ N}} \qquad (6.8)$$

However, as we discussed in the previous chapter, the electrostatic field of the drift cell causes non-isochronic charge collection. This creates a non-Gaussian tail in the electron arrival distribution, i.e. not all electrons can contribute to the 1-st electron timing because they arrive too late.

In addition, the electrons are produced in clusters, which cause additional variability in the ionization arrival. Table 1 shows the measurement of the cluster size distribution in percent for several gases [48]. Table 2 shows the ionization available per 1 cm of track length at 1 atm of pressure:

Table 2 - Primary and total ionization per cm at 1 atm (compilation of numbers taken from A.V. Zarubin [49], except the last three - taken from A. Pansky et al. [50]).

Gas	Primary ionization (clusters) [cm^{-1}]	Total ionization (electrons) [cm^{-1}]	Average energy needed to create one ion pair w [eV]	dE/dx (min) [keV/cm]
He	3.3	7.6	42.3	0.322
N_2	20.8	60.5	34.7	2.097
O_2	23.2	76.5	30.8	2.360
Ne	10.9	39.9	36.4	1.452
Ar	24.8	96.6	26.3	2.541
Kr	33	197.5	24.05	4.750
Xe	44.8	313.3	21.9	6.862
CO_2	33.6	100.0	32.8	3.280
CH_4	24.8	59.3	27.1	1.608
C_2H_6	40.5	117.7	24.4	2.870
iC_4H_{10}	83.6	232.8	23.2	5.402
DME	62	120 (?)	-	-
TEA	144	-	-	-
TMAE	281	-	-	-

Note: If the sample available for detection is only few mm long, we are dealing with rather small number of electrons available at 1 atm.

By including a correction for non-isochronous charge collection, gas pressure, and by assuming that E/p is constant while changing the pressure p, we can modify the equation (6.8):

$$\sigma_{diffusion}(1-\text{st arriving electron}) = \frac{0.91}{\sqrt{\ell n\,(\eta(x)\,N\,p)}}\,\frac{\sigma_L(1\ \text{electron})}{\sqrt{p}} \qquad (6.9)$$

where $\eta(x)$ is a correction describing the fraction of electrons, which can contribute to the first electron timing, x is the drift distance, p is the gas pressure, N is the total number of electrons per sample. Fig. 4 shows an example of the choice of gas pressure to control the drift chamber tracking resolution [51].

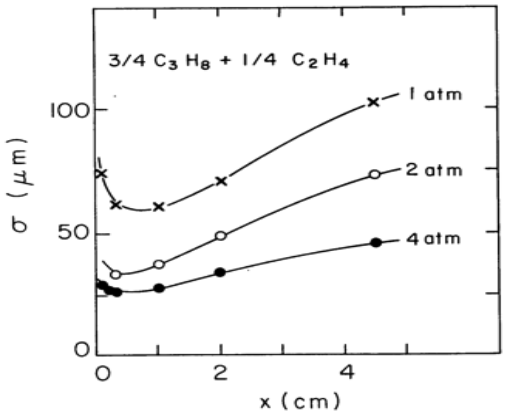

Fig. 4 - Chamber resolution as a function of pressure.

It is not straightforward to guess the $\eta(x)$ factor. One needs some knowledge of the charge collection, i.e. one needs a drift simulation program. In typical examples of high accuracy drift chambers the factor $0.91/\sqrt{\ell n\,(\eta(x)\,N\,p)}$ is close to 0.4-0.6 [38].

As an example, for the DME gas at 1 atm pressure, 1 cm sample size and 1 cm drift (consider the diffusion contribution only): in this case one has N ~ 120 electrons / cm, $\sigma_L(1\ \text{electron}) \sim 55\,\mu m/\sqrt{cm}$, $\eta(x) \sim 0.2$ (assume) and $0.91/\sqrt{\ell n\,(\eta(x)\,N\,p)} \sim 0.5$; therefore one could achieve resolution of about ~30 μm.

6.1.2. Center of gravity timing:

Let's assume that we have electronics capable of measuring every arriving electron. If we assume that the electron cloud is Gaussian then:

$$\sigma_{diffusion}(\text{center of gravity timing}) = \frac{1}{\sqrt{\eta(x)\,N\,p}}\,\frac{\sigma_L(1\ \text{electron})}{\sqrt{p}}, \qquad (6.10)$$

where $\eta(x)$ is the correction describing the fraction of electrons which are used for centroid timing; it is influenced by variables such as the geometry, speed of digitizing clock, method of analyzing data, etc. One can see, that now it would make more sense to invest into "being clever", i.e. to design the isochronous charge collection geometry.

The same example for the DME gas at 1 atm pressure, 1 cm sample size and 1 cm drift (consider the diffusion contribution only): in this case one has $\eta(x) \sim 1.0$ (assume an ideal case); therefore one could achieve resolution of about ~5 μm !!!

The Flash ADC digitizers came on the market ~15 years ago. Great improvements in resolution of high precision drift chambers were expected at that time. However, the hopes for an "ultra-high ~5 μm accuracy" short drift wire chambers did not materialize because of (a) non-isochronous charge collection, (b) fluctuation in the ionization statistics and (c) $\eta(x)$ factor is always less than one.

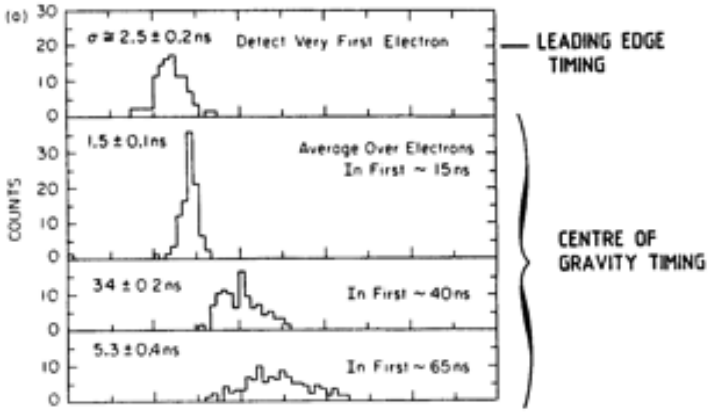

Fig.5 - Monte Carlo simulated resolution with a hypothetical infinitely fast electronics capable of digitizing every arriving electron in the jet chamber with 4 mm wire spacing, 90% Ar + 10% C_4H_{10} at 1 atm, B = 10 kG and 7.5 mm drift distance.

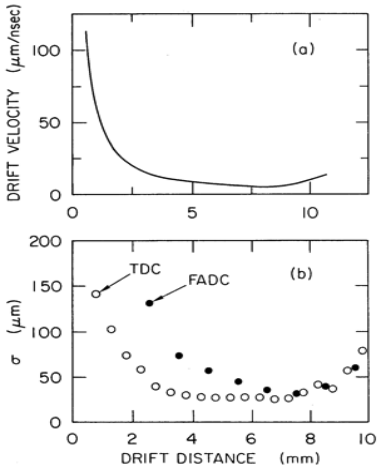

Fig.6 - Aachen Univ. drift chamber test; (a) drift velocity near the anode wire, (b) chamber resolution using the leading edge timing and center of gravity FADC timing.

Fig. 5 shows that the center of gravity timing is better than the 1-st electron timing only if we average over the electrons located in the near-isochronous central part of the sample. As we average over larger part of the sample the center of gravity is disturbed by the fluctuations in the ionization statistics coupled with the nonisochrony of the charge collection ($\eta(x) < 1$). In practice, of course, we do not have infinitely fast electronics. Closest practical approximation is the combination of a slow gas and the time expansion chamber, which uses extremely slow drift velocity. Fig. 6 illustrates that the centroid timing is actually worse than the leading edge timing if we are very close to the anode wire where the charge collection is very non-isochronous [52].

To average over the near isochronous limit means to use only the leading edge portion of the drift pulse, i.e. to use the first FADC bins of the pulse.

One should also remark that for the long drift distances (>10 mm) the FADC timing method gives finally better results than the leading edge timing method because the diffusion starts washing out the non-isochronous collections and the clustering effects.

6.3. Monte Carlo estimate

Example #1 - Mark II vertex chamber at SLC [53].

1. Assume the following drift chamber operating conditions:

92% CO_2 + 8% iC_4H_{10} gas at 4 atm pressure, tracks are either parallel to anode plane or 10° inclined, anode surface gradient $E_a \sim 450$ kV/cm at 2 atm and 590 kV/cm at 4

atm on the surface of 20 μm wire, the average drift field E ~ 2.1 kV/cm at 4 atm, giving an average drift velocity of about 4 μm/ns (slow gas) and magnetic field was off for this particular study.

2. Calculate the drift chamber pulses:

Creating first the weighted drift time distribution by:

a) Starting with a track segment assuming 3.4 clusters/mm of track (CO_2 gas). The probability distribution of electrons within each cluster is taken from argon data [53].

b) Stepping each electron in electrostatic field using the drift velocity and diffusion is determined at each point of the drift according to E/p at that point.

c) Assigning a weight x to each electron according to the Furry exponential distribution $A(x) \approx x \exp(-1.5x)$, to simulate the avalanche fluctuations.

3. The weighted drift time distribution is then convoluted with:

a) Response of the amplifier which is assumed to be a simple triangle with a 5 ns rise time and a 15 ns fall time.

b) Include the response of positive ions. This response, as we discussed earlier, has the form: $1/(1 + t/p\,t_0)$, where p is pressure, t is time and t_0 is the characteristic time. To improve the multiple hit capability, the design of the electronics minimized the pulse tail using so called zero-pole filter technique [55]. The zero-pole filters look as follows:

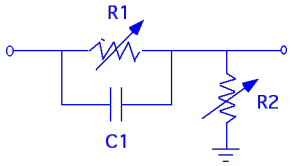

the design of these filters goes as follows. First, one has to express the "1 / t" tail in terms of three exponential curves:

$$\frac{1}{1+\frac{t}{p\,t_0}} = A\exp\left(-\frac{t}{\alpha\,p\,t_0}\right) + B\exp\left(-\frac{t}{\beta\,p\,t_0}\right) + C\exp\left(-\frac{t}{\gamma\,p\,t_0}\right) \qquad (6.11)$$

Notice that the first term is the "fast" term followed by two "slow" terms (A = 0.79, α = 1.6, B = 0.185, β = 13.5, C = 0.024, γ = 113.0, t_0 = 0.76 ns, p = 4 atm, $\mu(CO_2)$ = 1.09 cm^2 V sec^{-1}). One adjusts the components of the filter to cancel the middle term in equation (6.11). The resulting response is:

$$V(t) = 0.99\exp\left(-\frac{t}{\alpha\,p\,t_0}\right) + 0.01\exp\left(-\frac{t}{\gamma\,p\,t_0}\right) \qquad (6.12)$$

Fig. 7 shows the final drift pulse shape is calculated every 1 ns.

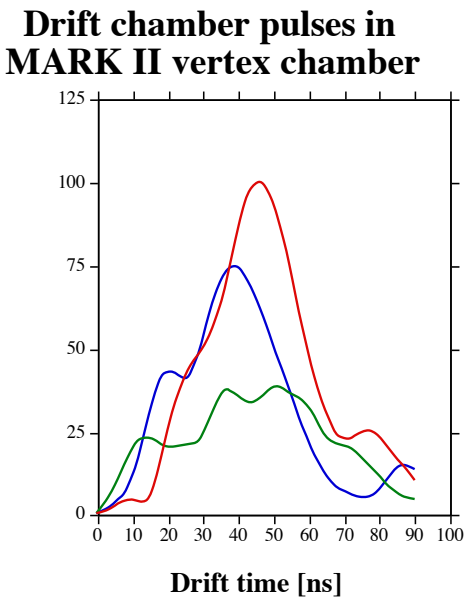

Fig.7 - Monte Carlo simulation of drift pulses in Mark II drift vertex chamber at SLC; 4 atm, 92% CO_2+8%iC_4H_{10} gas, v_{drift} = 4 μm/ns, 12 mm drift distance; 0^o angle in respect to wire plane.

3. Timing strategy with pulses of Fig.7:

a) The timing strategies with infinitely fast electronics which detects individual arrival times of each electron. This method can determine the limit of how well we can do.

b) The leading edge timing with the "realistic" pulses was obtained by fitting the first 5 points of the pulse waveform with the 3-rd order polynomial, we choose a threshold to be 2-3% of the average pulse peak, and then find the crossing point with the fitted curve.

c) The FADC centroid timing with the "realistic" pulses was done by assuming the 100 MHz clock, which determined the corresponding values on the waveform (every 10 ns). With these points one determines a simple center of gravity.

d) Other timing methods were tried: multiple threshold, the reference pulse timing for the FADC algorithm, the parabola fit, etc. None of them made an improvement in the above mentioned methods.

Table 1 - Simulated resolution in Mark II vertex chamber (4 atm in 92% CO_2+ 8% iC_4H_{10} gas, 12 mm drift) [53].

Timing method	Design (a) 0 degrees	Design (a) 10 degrees	Design (d) 0 degrees	Design (d) 10 degrees
First electron timing with infinitely fast electronics	20 ± 3 μm	34 ± 3	25 ± 2	32 ± 3
Centroid timing with infinitely fast electronics	7 ± 1	14 ± 2	12 ± 1	13 ± 1
Leading edge timing with realistic pulses (threshold ~2-3% of the average ampl.)	20 ± 3	48 ± 4	29 ± 2	36 ± 3
Centroid timing with the realistic pulses and 100 MHz digitizer	20 ± 1	27 ± 2	36 ± 3	43 ± 3

Table 2 - Simulated resolution in Mark II vertex chamber (2 atm in 92%CO_2+ 8% iC_4H_{10} gas, 12 mm drift)

Timing method	Design (a) 0 degrees	Design (d) 0 degrees
First electron timing with infinitely fast electronics	41 ± 4 μm	46 ± 4
Centroid timing with infinitely fast electronics	17 ± 2	21 ± 2
Leading edge timing with realistic pulses (threshold ~2-3% of the average ampl.)	41 ± 5	42 ± 5
Centroid timing with the realistic pulses and 100 MHz digitizer (use a simple centroid timing)	41 ± 3	42 ± 5

Experimental results from the vertex chamber of the Mark II experiment at SLC [56]:

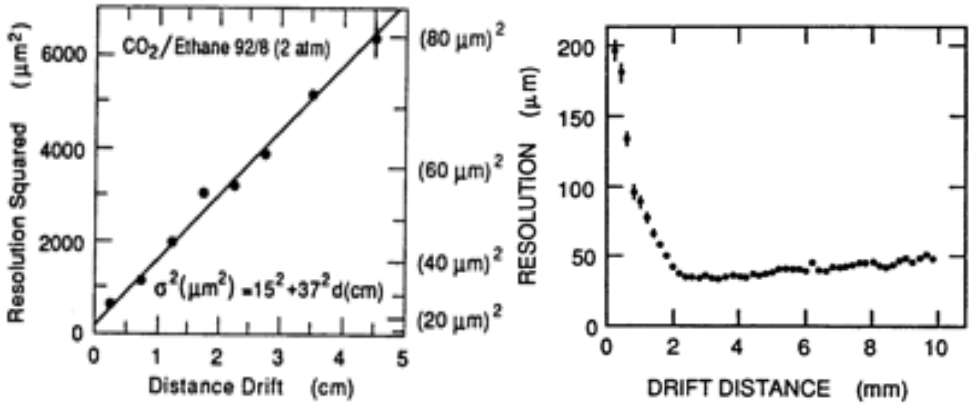

Fig.8 - Measured tracking resolution in Mark II vertex chamber in the middle of drift cell at 2 atm.

Fig.9 - Measured tracking resolution in Mark II vertex chamber near the anode wire at 2 atm.

The resolution in the middle of the drift cell follows the well known diffusion law: $\sigma(\mu m) = \sqrt{15^2 + 37^2\, d(cm)}$, i.e. 46 ± 4 μm for 12 mm drift distance and 2 atm pressure, which is close to the Monte Carlo prediction (41 ± 5 μm) [53] - see Figs. 8 and 9.

Studies with various timing "tricks" to improve the accuracy were considered studying the micro-jet chamber prototype for possible use at HRS [57]. However, in this particular case, where one deals with short drift distances, the first electron timing was the best result on could achieve.

Radial drift chamber

All previously mentioned methods either used only a small portion of the ionization available or were sensitive to clustering effects.

D. Nygren suggested a technique to utilize all available ionization with equal weight and be insensitive to the clustering effect [58] - see Fig. 13. One should note that A. H. Walenta proposed similar concept called "induction" chamber [59].

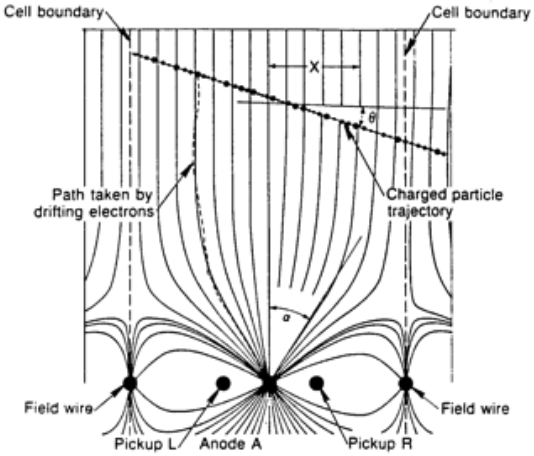

Fig.13 - Principle of the radial drift chamber.

The drift is radial using the low diffusion DME gas. Each electron's original position is reconstructed by measuring both drift time and angle α using two avalanche charge pick-up electrodes L&R - see Fig. 13. One expects $\eta(x) \sim 1$ in equation (6.10), i.e. $\sigma_{diffusion}(\text{center of gravity timing}) \sim 55/\sqrt{120} \sim 5\,\mu m$ for DME gas.

D. Nygren's analysis of a practical chamber design operating with DME gas at 1 atm (total ionization in DME is N= 120/cm, $\sigma_{diffusion} \sim 55\,\mu m/\sqrt{cm}$), N_S=10 is the number of samples per cm, $\langle N_e \rangle$= 12 is the average number of electrons per sample, $\sigma_{el.} \sim 20\,\mu m$ is the

electronics noise, $\sigma_{aval.} \sim 88\ \mu m$ is the r-ϕ avalanche noise and radial distance of 3 cm with 30 samples. This appears to be the best one can do with a gaseous detector.

$$\sigma_{r-\phi} = \sigma_{el.} \oplus \frac{\sigma_{diffusion}}{\sqrt{< N_e >}} \oplus \frac{\sigma_{aval.}}{\sqrt{< N_e >}} = 20 \oplus \frac{55}{\sqrt{12}} \oplus \frac{88}{\sqrt{12}} \sim 36\ \mu m \text{ per sample}$$

$$\sigma_z = \sigma_{el.} \oplus \frac{\sigma_{diffusion}}{\sqrt{< N_e >}} = 20 \oplus \frac{55}{\sqrt{12}} \sim 25\ \mu m \text{ per sample}$$

Chapter 7

7.1. Wire ageing

The avalanche creates a plasma condition which induces the polymerization process. To get a introduction to the problems involved, I recommend to read two reviews about this subject by J. Va'vra [60] and J. Kadyk [61].

Physicist's view of the avalanche: **Chemist's view of the avalanche:**

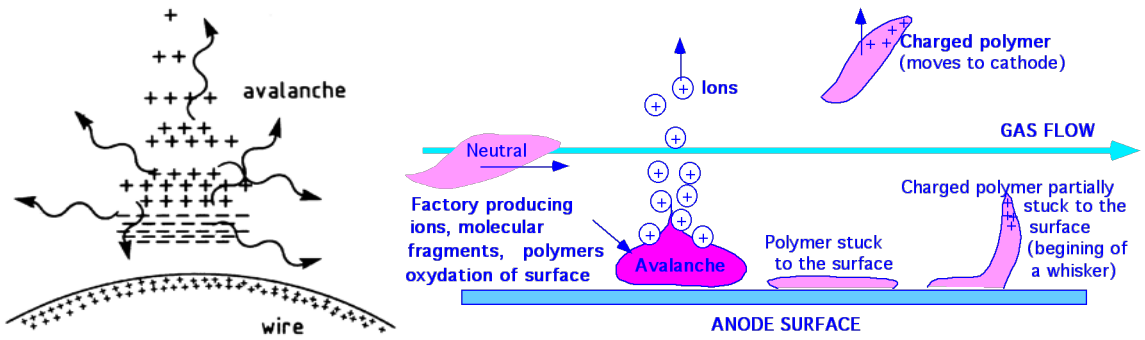

7.1.1. Anode related problems.

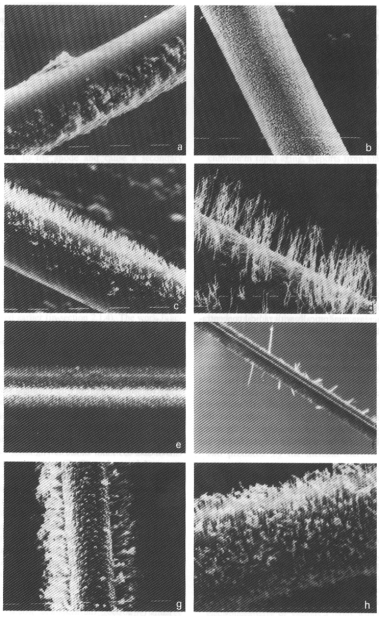

Fig.1 Whisker formation [61].

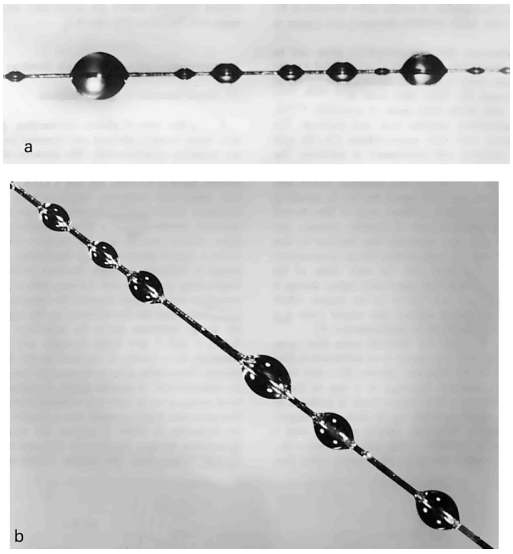

Fig. 2 Film / liquid droplet formation [62,63]

For example, droplets were observed on anode wires in CH_4 + TMAE after obtaining a charge dose ~5-10 mC/cm, and then exposing the chamber to air - see Fig. 2.

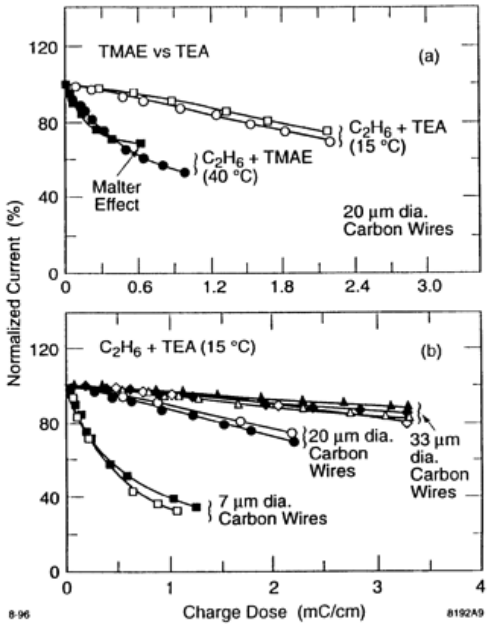

Fig. 3 Dependence on the anode wire diameter and some specific molecule [64].

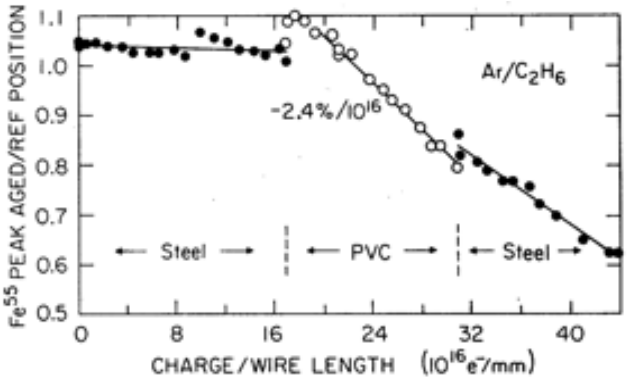

Fig. 4 Dependence on the gas tubing material [65].

General comments about wire ageing:

1. It is a very complicated chemical process, which is not well understood quantitatively, except in few isolated cases.

2. However, what is already very clear is that one should:

a) build the wire chambers as cleanly as possible,

b) avoid soft glues or outgasing materials,

c) test all materials used in the construction under the most representative condition - see Fig. 4.

3. The ageing rate depends on:

a) wire radius (smaller radius larger gain drop) - see Fig. 3,

b) wire alloy (oxidation of surfaces),

c) gas type -see Fig. 3,

d) gas additive (water, alcohol, etc.),

e) gas flow,

f) gas pressure, etc.

4. What to do about the wire ageing problem:

a) wire replacement,

b) wire washing in alcohol (TMAE ageing),

c) wire heating (TMAE ageing),

d) run the gas gain as low as possible (preventive),

e) limit the charge doses by making the detectors thin (preventive).

7.2. Cathode related problems

7.2.1. Malter effect [66,67] - see Fig. 5:

Discharging time constant is RC $\sim \varepsilon_r \varepsilon_0 \rho_{film}$, where $\varepsilon_r \sim 4$, $\varepsilon_0 \sim 8.85$ pF/m, $\rho_{film} \sim 10^{12}$ - 10^{15} $\Omega \bullet$ cm => For $\rho_{film} \sim 10^{15}$ $\Omega \bullet$ cm the time constant is RC~ 15 min.

If the radiation source is present, there is going to be a charge build up on the surface of the insulator, and one can reach a very high gradient across the thin insulator film. This can cause the electron emission which can lead to a positive feedback mechanism:

a) The Malter effect shows up as a continuous current present even when the source is removed.

b) or only occasional sporadic bursts [68].

7.2.2. Photo-cathode damage - see Fig.6:

The damage can be caused by [69]: a) sparking, b) environmental damage, c) electrolytic currents within the photo-cathode material, d) light exposure, e) gas gain. Example of a damage by an operation with gas gain [70] can be seen in Fig. 6. All photosensitive materials and their ageing by-products are good insulators. Therefore they could suffer from the Malter effect.

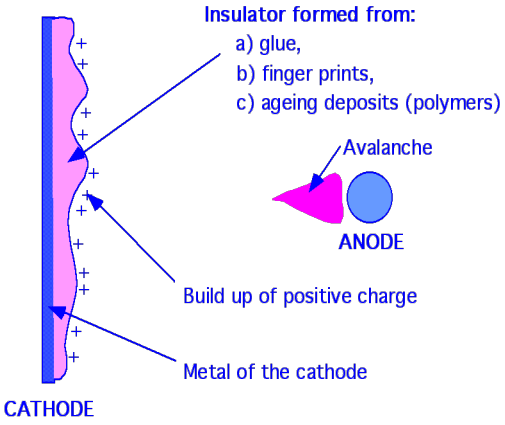

Fig. 5 Malter effect origin.

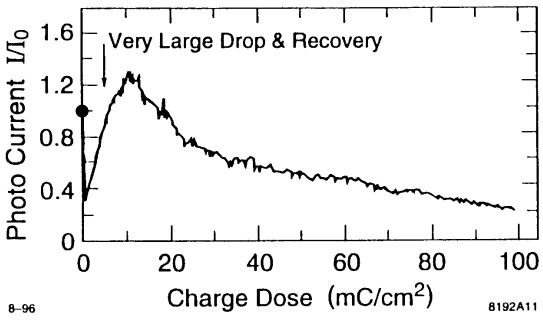

Fig. 6 Aging of CsI [70].

7.3. Quenching problems

Avalanches produce photons which have to be absorbed by the hydrocarbon molecules, which have many vibrational modes.

Example of extremely bad quenching is CF_4 + TMAE gas. The avalanche excited CF_4 molecule emits photons at 170 nm, which are capable of photoionizing the TMAE molecule. This results in an extremely unstable operation where an avalanche breeds secondary avalanches [71] - see Fig. 7.

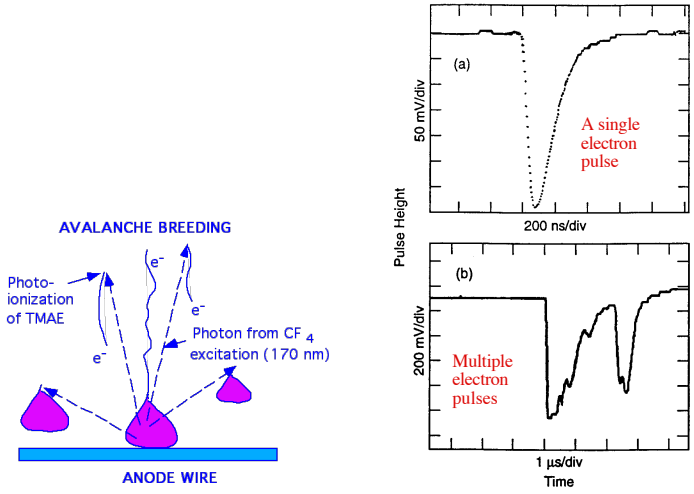

Fig. 7 Avalanche breeding.

One can also photo-ionize the nearby surfaces, which may have been coated by the polymerization products.

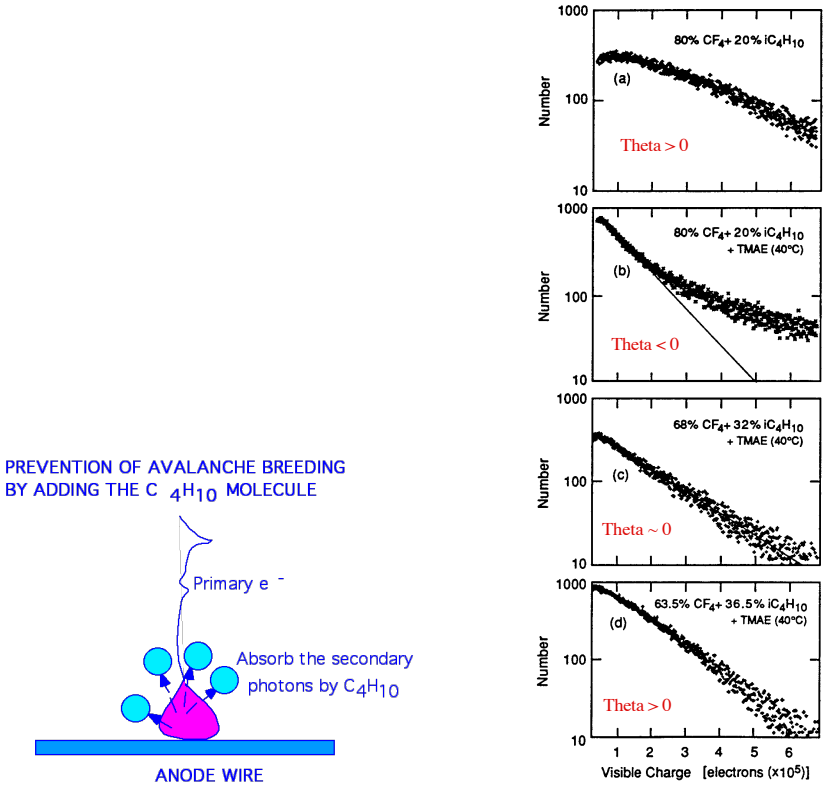

Fig. 8 Avalanche breeding can be stopped by an addition of C_4H_{10}.

The avalanche breeding can be recognized by observing an excessive tail in the single electron pulse height distribution resulting in the negative θ parameter in the Polya function. To fix the problem of avalanche breeding, one has to add a C_4H_{10} molecule which absorbs the 170 nm photons [71]. - see Fig. 8.

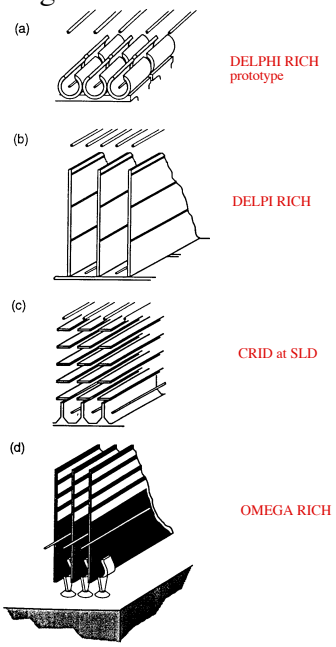

Fig. 9 An attempt to shield avalanche photons.

To be able to detect the single electrons, the chambers used a relatively high gas gain (2-3x10^5); people built "barricades" (see Fig. 9) around the anode wires to limit the photon feedback in a presence of large dE/dx track deposits [72]. A real fix is to run lower gas gain and make the detectors thin.

7.4. High voltage problems

a) **Sparking condition** [73]:

$$N_{\text{primary ionization deposit}} * G > 10^8$$

where $N_{\text{primary ionization deposit}}$ is the total primary ionization deposit, G is the average gas gain. A consequence of this law is that the α-particles may cause sparking sooner than the minimum ionizing particles for the same gas gain. This explains why sometime a chamber works in the lab and not in a real background environment next to the beam line !!

b) **High voltage insulation using several insulating layers**.

A bad HV design is a combination of G-10 sheet and Kapton printed circuit - see Fig. 10. There will be always some pin hole in Kapton causing a spark !!

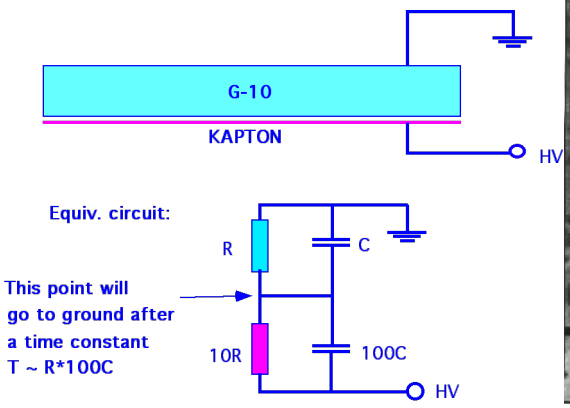

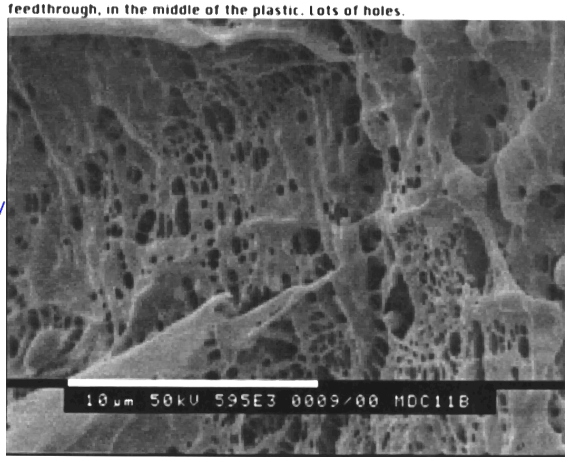

Picture taken by R. Malchow, Col. St. Univ.

Fig. 10 Example of bad HV design. **Fig. 11** Voids in Delrin coasing a current leakage.

c) **Delrin pins in large drift BES chamber.**

As a result of not following the DuPont Co. molding procedure, the feedthrough developed the high voltage problem after several months of running - see Fig. 11.

7.5. Sensitivity to various drifts :

1. **Gas mixture changes:**	**Change**	$\frac{\Delta PH}{PH}[\%]$
90% Ar + 10% CH_4	Δ Ar = 1%	11
90% Ar + 10% CO_2	Δ Ar = 1%	10
50% Ar + 50% C_3H_8	Δ Ar = 1%	5
2. **Barometric pressure change**s (EPI):		
95% Ar + 5% CH_4	Δ P = 1%	7
3. **Leaks** (MAC at PEP I):		
86% Ar + 14% CH_4	add 0.6% of N_2	10
86% Ar + 14% CH_4	add 0.15% of O_2	10
4. **Voltage drifts** (JADE):		
90% Ar + 10% CH_4	ΔV_{gain} = 1%	20
90% Ar + 10% CH4	ΔV_{drift} = 5%	25

References:

1. F . Sauli, CERN Yellow Report 77-09, 1977.
2. D.H. Wilkinson, "Ionization chambers and counters," 1950.
3. W. Blum and L. Ronaldi, "Particle detection with Drift Chambers," Spring-Verlag, 1994.
4. P.M. Morse and H. Feshbach, Methods of theoretical physics, McGraw Hill, New York, 1953.
5. R. Venhof, Drift Chamber Simulation Program GARFIELD, CERN/DD Garfield Manual, 1984.
6. K.J. Binns and P.J. Lawrenson, "Analysis and computation of electric and magnetic field problems," Pergamon Press, 1973, p.241.
7. S. Yellin, CRID note #40, SLD, SLAC, April 4, 1988.
8. S. Parker, Nuclear Instr.&Meth., A275(1989)494.
9. R. Bellazzini and M.A. Spezziga, Rivista Del Nuovo Cimento, Vol.17, N.12, 1994.
10. H.J. Burckhart et al., Nuclear Instr.&Meth., A244(1986)416.
11. J. Va'vra, Mark II Vertex chamber internal note, SLAC, February 2, 1985.
12. J. Va'vra, BaBar Internal DC note, SLAC, April 19, 1993.
13. I.R. Boyko et al., Nuclear Instr.&Meth., A367 (1995) 321.
14. L. Tonks, Phys. Rev. 97(1955)1443.
15. T. Kunst, B. Goetz and B. Schmidt, Nuclear Instr.&Meth., A324(1993)127.

16. P. Coyle et al., SLAC-PUB-4403.
17. K. Abe et al., Nuclear Instr.&Meth., A343 (1994) 74.
18. B. Schmidt, Dissertation, Univ. of Heidelberg, 1986.
19. G. Schultz and Gresser, NIM 151(1978)413, and G. Schultz, Ph.D. thesis, 1976.
20. L. G. H. Huxley and R.W. Crompton, "The diffusion and drift of electrons in gases."
21. K.F. Ness and R.E. Robson, Phys. Rev A, 34(1986)2185.
22. P.Coyle, Lorentz program.
23. S. Biagi, Nuclear Instr.&Meth., A273(1988)533 (available as MAGBOLTZ program).
24. H. Pruchova and B. Franek, Nucl. Instr&Meth., A366(1995)385; Issue of ICFA Bulletin, SLAC-PUB-7376, 1997; and H. Pruchova's Ph.D. thesis, Prague Tech. Univ.
25. J. Groh, Interner Bericht DESY FH1T-89-03 May 1989.
26. M. Matobe et al., IEEE Trans. Nucl. Sci. NS-32,541(1985).
27. Diethorn, USAEC Report NY06628 (1956).
28. Zastawny, J. Sci. Instrum., 1966, Vol. 43, p.179.
29. S.A. Korff, "Electrons and Nuclear counters," 1955.
30. P.G. Datskos, J.G. Carter, L.G. Christophorou, J. Appl. Phys. 71(1992)15.
31. S. Biagi, Nucl. Instr. & Meth.. A310 (1991) 133.
32. Byrne, Proc. R. Soc. Edinburgh 66A(1962)33.
33. Raether, "Electron Avalanches and Breakdowns in Gases," Butterworths, London, 1964.
34. Schlumbohm, Z. Phys. 151 (1958)563.
35. J.Va'vra et al., Nuclear Instr.&Meth., A324(1883)113.
36. Y. X. Wang, G. Godgrey, Nuclear Instr.&Meth., A320 (1992) 238.
37. J. Va'vra, CRID note #50, SLD, SLAC, 1987.
38. J. Va'vra, Nuclear Instr.&Meth., A244(1986)391 and Nuclear Instr.&Meth., 225(1984)445.
39. P. Bock, OPAL, Heidelberg Univ., 1984, unpublished.
40. S. Ramo, Proc. I.R.E. 27(1939)584.
41. J. Va'vra, SLAC-PUB-2635, October 1980.
42. R.B. Owen and M.L Awcock, IEEE Trans. Nucl. Sci, NS-15 (1968) 290.
43. C.F.G. Delaney, Electronics for the Physicist, Ellis Horwood, Chichester, West Sussex, UK, 1980.
44. J. Va'vra, SLD, CRID note #75, Nov. 24, 1992, D. Aston et al., Nucl. Instr. & Meth. A283 (1989) 590, and K. Abe et al., Nuclear Instr.&Meth., A343(1994)74.
45. F. Villa , Nuclear Instr.&Meth., A217(1983)273.
46. S. Bobkov et al., CERN-EP/83-81.

47. Cramer, "Mathematical Methods of Statistics," Princeton Univ. Press 1951.
48. Fischle et al., Nuclear Instr.&Meth., A301 (1991) 202.
49. A.V. Zarubin, Nuclear Instr.&Meth., A283 (1989) 409.
50. A. Pansky et al., Nuclear Instr.&Meth., A323 (1992) 294.
51. W. Farr et al, NIM 154 (1978) 175.
52. V. Commichau et al., Aachen Univ. preprint, PITHA 84-34.
53. J. Va'vra, SLAC, Mark II vertex chamber internal notes Oct. 12, 1984 and Oct. 31, 1984; and summarized in Nuclear Instr.&Meth., A244 (1986) 391.
54. F. Piuz, Nuclear Instr.&Meth., 175 (1980) 297.
55. Boie et al., Nuclear Instr.&Meth., 192(1982)365.
56. D. Durrett et al., SLAC-PUB-5259, May 1990.
57. J.Va'vra, Nuclear Instr.&Meth., 217(1983)322 and Nuclear Instr.&Meth., 225(1984)445.
58. J. Huth and D. Nygren, TPC-LBL-85-7.
59. A. H. Walenta, SLAC-PUB-259, 1982.
60. J. Va'vra, Nuclear Instr.&Meth., A252(1986)547.
61. J. Kadyk, Nuclear Instr.&Meth., A300(1991)436.
62. J. Va'vra, IEEE Trans.Nucl.Sci. NS-35, 1(1987)487.
63. C. Woody, IEEE Trans. Nucl. Sci. NS-35, 1(1988)493.
64. J. Va'vra, Nuclear Instr.&Meth., A387(1997)183.
65. Kothaus, LBL workshop, Berkeley, 1986.
66. L. Malter, Phys. Rev. 50(1936).
67. Guentherschultze, Z. Phys. 86(1933)778.
68. J. Va'vra, Nuclear Instr.&Meth., A367(1955)353.
69. P. Krizan et al., Nuclear Instr.&Meth., A387(1997)146.
70. A. Breskin, Nuclear Instr.&Meth., A371 (1996)116.
71. J.Va'vra et al., Nuclear Instr.&Meth., A370 (1996) 352.
72. J. Va'vra, Nuclear Instr.&Meth., A371 (1996) 33 and Nuclear Instr.&Meth., A387(1997)137.
73. H. Raether, Z. Phys. 112(1939)464.